

Coupling boreal forest CO₂, H₂O and energy flows by a vertically structured forest canopy – Soil model with separate bryophyte layer

Samuli Launiainen ^{a,*}, Gabriel G. Katul ^b, Ari Lauren ^a, Pasi Kolari ^c

^a Natural Resources Institute Finland, Environmental Impact of Production, Vantaa, Finland

^b Nicholas School of the Environment and Earth Sciences, Duke University, Durham, NC, USA

^c University of Helsinki, Department of Physics, Helsinki, Finland



ARTICLE INFO

Article history:

Received 18 November 2014

Received in revised form 25 May 2015

Accepted 3 June 2015

Keywords:

Boreal forest

Multi-layer SVAT model

Moss layer

Energy exchange

Gas exchange

Soil water balance

ABSTRACT

A 1-dimensional multi-layer, multi-species soil-vegetation-atmosphere transfer model APES (Atmosphere-Plant Exchange Simulator) with a separate moss layer at the forest floor was developed and evaluated for a boreal Scots pine forest situated in Hyttiälä, Southern Finland. The APES is based on biophysical principles for up-scaling CO₂, H₂O, heat and momentum exchange from canopy element level to a stand scale. The functional descriptions of sub-models were parametrized by literature values, previous model approaches and leaf and moss gas exchange measurements, and stand structural characteristics derived from multi-scale measurements. The model was independently tested against eddy-covariance fluxes of CO₂, H₂O and sensible heat measured above and within the canopy, and against soil heat flux and temperature and moisture profiles. The model was shown to well reproduce fluxes and resulting scalar gradients at diurnal and seasonal timescales. Also predictions for moss moisture content and soil moisture and temperature dynamics were acceptable considering the heterogeneity in soil hydraulic and thermal properties and uncertainties in boundary conditions.

The model framework allows for (1) coupling above-ground with the soil domains through the feedbacks between soil water and vegetation mediated by the moss layer, (2) several vascular plant species or cohorts in a multi-species canopy, and (3) explicit treatment of bryophyte layer energy and water balance and bottom layer – atmosphere exchange. These features make APES well-suited for exploring feedbacks between boreal forest structure, site conditions and vegetation processes controlling ecosystem-atmosphere exchange.

© 2015 Elsevier B.V. All rights reserved.

1. Introduction

Being the largest biome globally, boreal forests have direct effects on regional and global climate through absorption of solar radiation and momentum, and partitioning of the net radiation into sensible *H* and latent heat *LE* (Bonan, 2008; Chapin et al., 2000; Law et al., 2002; Baldocchi, 2008; Baldocchi et al., 2000). Their appreciable carbon dioxide uptake from the atmosphere and influence on biogenic aerosol formation are now rarely disputed (Malhi et al., 1999; Mäkelä et al., 1997; Spracklen et al., 2008). Temporal variations in the structure and function of boreal forests occur at multiple scales, from seconds (e.g. radiation regime inside the canopy, leaf gas exchange, turbulent flow) to seasonal (phenology, annual cycle of functional substances) and longer (stand age, species composition, management). Spatial variability among stands is commonly

associated with gradients in the climate and site type, which in turn, affect species composition and stand structure. Also, forest management does have major impacts on such forests thereby drawing significant research interest in the interplay between silviculture and the role of boreal forests in climate regulation (Esseen et al., 1997; Bengtsson et al., 2000).

Plant carbon uptake, water use and energy exchange with the atmosphere in response to environmental variations remains complex and governed by multiple interactions and feedbacks. Changes in structure and function of boreal forests affect within-canopy and soil micro-environment that then impact the rates of carbon dioxide (CO₂), water (H₂O), heat and momentum exchanges occurring within and between canopy elements as well as soil layers. When spatially integrated, these alter the bulk exchange rates between the forest ecosystem and the atmosphere as well as water, carbon and nutrient flows in catchments. Considering water and carbon fluxes in the forest stand for instance, increase of overstory leaf area leads to greater amount of precipitation being intercepted, resulting in a decreased throughfall and soil infiltration. Simultaneously,

* Corresponding author. Tel.: +358 29 532 5323.

E-mail address: samuli.launiainen@luke.fi (S. Launiainen).

absorption of radiation is enhanced and carbon uptake and transpiration rates from the overstory are expected to increase leading to more rapid depletion of soil water within the root zone. In coarse-textured sites, this depletion increases the probability of 'ecological drought', i.e. water deficits in the root zone, that can then modify a plethora of processes related to tree responses to climate variation, forest floor fluxes and soil processes (Skre and Oechel, 1981; Vargas et al., 2010; Williams et al., 2012; Katul et al., 2012; Zhou et al., 2013).

Delineating the causes and projecting the responses of forest ecosystems to changing environmental conditions and management requires mathematical models that describe the interplay between forest structure, micro-climate and site conditions. In canvassing available methods for representing the soil-plant-atmosphere system, the level of details within and across various compartments can be daunting and often un-balanced. For example, 3-D models of water flow in the soil-root system have been used for quite some time to describe water uptake where root-distribution and morphology is known at different resolution (Couvreur et al., 2012; Doussan et al., 2006; Siqueira et al., 2008; Simunek and Hopmans, 2009; Manoli et al., 2014). Often, such models remain primitive in their treatment of above-ground processes. Likewise, 3-D radiation models have been developed and linked to photosynthesis when spatial heterogeneity in the light environment is large (Cescatti and Zorer, 2003; Cescatti, 1997), but again, these models commonly ignore below ground-processes altogether. Other approaches that seek maximum simplicity represent the entire canopy as a single layer (big-leaf) and the entire soil-root system in a lumped layer (Porporato et al., 2004). This approach clearly misses potentially significant gradients in the micro-environment (both above and below ground) that non-linearly interact with layer-wise sources and sinks (Juang et al., 2008).

Due to absorption of solar radiation and momentum, the largest micro-climatic gradient in vegetation canopies occurs vertically, necessitating, at minimum, 1-D multi-layer soil-vegetation-atmosphere transfer models (SVAT's). Common to the multi-layer models is that they assume the planar gradients in mass, heat, and energy fluxes and micro-climatic state variables small when compared to vertical inhomogeneities across the entire canopy height. By combining canopy radiation schemes and eco-physiological principles with turbulent transport representation, they enable predictions and independent verification of stomatal and other pathways by which CO₂, water vapor, and other scalars are exchanged between leaves, canopy elements and the atmosphere across various levels within the canopy volume (Meyers and Baldocchi, 1988; Harley and Baldocchi, 1995; Leuning et al., 1995; Baldocchi and Meyers, 1998; Ogée et al., 2003; Juang et al., 2008; Olchev et al., 2008).

The utility of such model framework is that relying on quantitative biophysical representation of canopy and soil processes, most of which can be independently parametrized and verified, enables direct up-scaling from element to stand scale (and beyond). However, significant challenges still remain when describing feedbacks between the above-ground and soil domains and resolving the vegetation functioning and root water and nutrient uptake under non-optimal soil water conditions (Simunek and Hopmans, 2009; Manzoni et al., 2010; Markewitz et al., 2010; Katul et al., 2012; Zhou et al., 2013; Volpe et al., 2013). Neither are the moss layer processes in boreal ecosystems sufficiently described (Stoy et al., 2012). This layer has a fast response time scale associated with radiation fluctuations at the forest floor, an intermediate time scale response associated with drying of the soil, and a slow response time scale associated with the dynamics of stand leaf area. Addressing the above challenges require models that enable species-specific representation of atmosphere-plant exchange (Ogée et al., 2003; Olchev

et al., 2008; Flerchinger et al., 2009) that is becoming possible through leaf-scale data collected to plant trait databases such as TRY (Kattge et al., 2011).

In this work, a parsimonious treatment of below and above ground processes using a 1-D multi-layer, multi-species forest canopy – soil model labeled APES (Atmosphere-Plant Exchange Simulator) that accounts for the vertical structure and functional diversity of boreal forests is proposed. The APES describes the main structural and functional compartments of a boreal forest ecosystems accommodating the effects of vascular plant species and the bryophyte layer at the forest floor as well as their interactions with the forest soil and canopy microclimate. Formulations in each layer (soil, plant or canopy air space) reflect a trade off between desirable traits of realism and simplicity. We first describe the model theory along with how its parameters are estimated. Then, we evaluate the APES predictions against ecosystem-scale CO₂, H₂O and energy fluxes and environmental data measured in a Scots pine stand at the Hytylä SMEAR II-station in Southern Finland. Finally, we consider the soil controls on leaf gas-exchange and bottom layer processes. In future studies, the APES is used to disentangle the leaf-area, species, soil and silvicultural controls of boreal forest H₂O, CO₂ and energy exchange.

2. Model framework

In APES, the main compartments of the forest stand are described as objects that include the governing conservation equations and contain structural and functional description of the respective part of the ecosystem (Fig. 1). The independent objects and sub-models are then linked by physical transport processes, formulated using gradient-diffusion approximations

$$f_s = -K_i \frac{\partial s}{\partial z} = g_i \Delta s, \quad (1)$$

that links flux f_s to local gradient of s ($\partial s / \partial z$) using an exchange coefficient or conductivity K_i , or bulk conductance g_i .

The above-ground airflow sub-model represents the canopy as a horizontally homogenous porous medium, where canopy elements are randomly distributed in horizontal space. The canopy structure is primarily accounted through a vertical leaf-area density distribution $\Lambda_{l,t}(z)$ (m² m⁻³) satisfying the normalizing condition $LAI = \int_0^h \Lambda_{l,t}(z) dz$, where LAI is the leaf area index and h is the canopy height. The transfer and absorption of shortwave and longwave radiation, transport of scalars and momentum and partitioning of rainfall between interception and throughfall also occurs in these canopy layers, impacted by $\Lambda_{l,t}(z)$.

The forest *Canopy* object consists of one or several *PlantTypes*, which may be vascular plant species, functional groups or age cohorts distinguished by their structural properties, such as leaf or root area densities, height and leaf size, and/or by physiological characteristics such as phenology, photosynthetic capacity and stomatal conductance. Leaf gas and energy exchange is calculated separately for sunlit and shaded leaves using well-established iterative solution of coupled photosynthesis-stomatal conductance theories (Farquhar et al., 1980, 2001; Katul et al., 2010; Medlyn et al., 2012) and leaf energy balance. Solutions of soil water and heat transfer in the *SoilProfile* object are linked to physiological controls at the leaf level, and root water uptake is described by a macroscopic multi-layered root model (Volpe et al., 2013). A separate *BottomLayer* object describes water, energy and CO₂ dynamics in the bryophyte layer at the forest floor.

As time-dependent forcing variables, APES uses time-averaged (usually 1/2 hourly) meteorological variables at a reference level above the canopy. These variables include direct and diffuse photosynthetically active (Q_p) and near-infrared (Q_n) radiation, mean

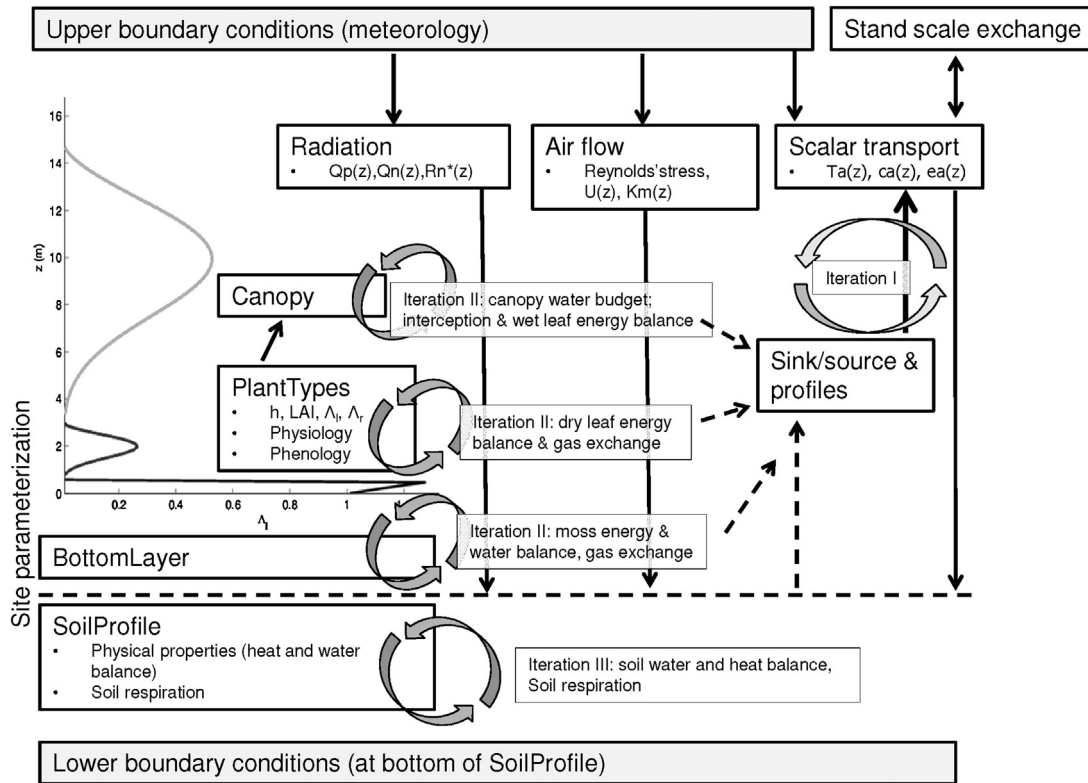


Fig. 1. Conceptual diagram of APES, and leaf-area density profiles Λ_l used for the SMEAR II-site.

wind speed U (or friction velocity u_*), precipitation rate P , mean air temperature T_a , and mixing ratios of H_2O and CO_2 . In addition, appropriate lower boundary conditions for soil water and heat flow below the rooting zone need to be specified. The APES captures many of the non-equilibrium thermodynamic aspects of the soil-plant-atmosphere system (i.e. the soil-leaf-atmosphere temperature gradients, radiation and heat are exchanged within and among components). However, APES assumes stationary conditions for the fast above ground processes associated with turbulent transport and radiation attenuation. Any temporal variability in those processes originates from variability in meteorological variables (i.e. boundary conditions). However, for the slowly evolving forest floor and soil processes, the continuity equations describing heat and mass transport are treated as unsteady.

To resolve the interaction between canopy processes and microclimate, the solution of mass and energy exchanged during a timestep Δt consists of three iteration loops summarized as (Fig. 1):

- (1) Within-canopy profiles of $U(z)$, eddy diffusivity K_s and incident and absorbed shortwave radiation are calculated.
- (2) Initializing T_a , H_2O and CO_2 profiles in the canopy air space by setting them equal to their forcing values at the highest grid-point (vertically uniform conditions within the canopy). This assumption amounts to assuming turbulence levels are sufficiently large so that the air within and near the canopy top is sufficiently well mixed yielding constant T_a , H_2O and CO_2 with z but not time (as a first guess).
- (3) Calculating scalar sink/source term Σ_S within the canopy (Iteration II). This includes (i) net isothermal radiation; (ii) interception of precipitation and subsequent evaporation from wet parts of a canopy layer; (iii) dry leaf energy balance and gas exchange, computed separately for each *PlantType* and each layer; (iv) calculation of *BottomLayer* energy, H_2O and CO_2 exchange.

- (4) Updating mean scalar concentration profiles in the canopy air space and repeating steps (2) and (3) until convergence of all scalars and layers (Iteration I). During Iterations I and II, values of the slowly evolving soil state variables are taken from the previous time step.
- (5) Solving soil water and heat flow (Iteration III) and updating volumetric water content θ , soil temperature T_s and soil respiration R_s .

A general description of the model is presented next while the specific parametrization for boreal coniferous forest is described in Section 3.

2.1. Canopy microclimate and upscaling

2.1.1. Short and longwave radiation

Above the canopy, the downward solar radiation consists of a direct beam $Q_{b,0}$ incident at a zenith angle Ψ and a downward diffuse $Q_{d,0}$ radiation originating from the whole hemisphere with equal intensity. The probability that direct radiation penetrates a canopy layer i (numbered from top of the canopy) without being intercepted is

$$\tau_{b,i} = \exp \left[-K_b(\Psi) \Omega \Lambda_{l,t}(z_i) dz \right], \quad (2)$$

where $\Lambda_{l,t}(z_i)$ ($m^2 m^{-3}$) is the one-sided (hemisurface) leaf area density of all *PlantTypes* in the layer i and $\Omega \Lambda_{l,t}(z_i)$ determines 'effective' leaf area in terms of radiation transfer through a combined shoot- and tree-scale clumping-factor Ω (–). The beam extinction coefficient K_b (–) represents the mean leaf projection per unit leaf area in the direction of the radiation, calculated based on ellipsoidal leaf-angle distribution (Campbell and Norman, 1998). The intercepted part $(1 - \tau_{b,i})$ of Q_b is either absorbed, transmitted through the plant elements and segregated to downward hemispherical (diffuse) flux Q_d , or reflected upwards to become upward

radiation Q_u . In the canopy layers, the diffuse components behave similarly to Q_b but the probability $\tau_{d,i}$ for passing without being intercepted through layer i is obtained by integrating Eq. (2) over the hemisphere. Inside canopies, $Q_{d,i}$ consists of two parts: the part of $Q_{d,0}$ from the sky that has penetrated to layer i without being intercepted, and the part that has resulted from series of multiple reflections and transmissions between the canopy layers and the forest floor. Multiple scattering processes also contribute to Q_u . At the canopy top, the ratio of Q_u to incoming radiation ($Q_{b,0} + Q_{d,0}$) defines the canopy albedo (Zhao and Qualls, 2005).

The profiles of incident Q_b , Q_d and Q_u (Wm^{-2} (ground)) within the canopy are computed separately for photosynthetically active (PAR) and near-infrared (NIR) wavebands using a multi-layer radiation transfer model including multiple scattering among the vegetation layers and between the canopy and forest floor (Zhao and Qualls, 2005), and only modifications for clumped coniferous canopies are presented. Following Ni-Meister et al. (2010), a single conifer shoot is considered as the basic scattering element, and a shoot albedo is related to needle single-scattering albedo α_l via $\alpha \simeq \alpha_l \frac{4\overline{\text{STAR}}}{1 - \alpha_l(1 - 4\overline{\text{STAR}})}$, where $\overline{\text{STAR}}$ is the shoot silhouette to total area ratio (0.1–0.2 for Scots pine, Smolander et al., 1994). For simplicity the Ω and α (within a given waveband) are taken constant neglecting their vertical variations in the canopy or between *PlantTypes*. Also contribution of woody plant parts on radiation interception are neglected, a fair assumption for the coniferous ecosystem considered here. The relative probabilities of forward and back-scattering are set to 0.4 and 0.6, respectively (Zhao and Qualls, 2005).

At each canopy layer, the absorbed radiation $Q_{a,t}$ is the difference between radiation entering and leaving the layer. When the leaves are separated into sunlit sl and shaded sh fractions, $Q_{a,t}$ must satisfy a normalizing condition

$$Q_{a,t} = [\xi_{sl}Q_{sl} + (1 - \xi_{sl})Q_{sh}] \Lambda_{l,t} dz, \quad (3)$$

where the fraction of sunlit foliage $\xi_{sl,i}$ is smaller than τ_b due non-random distribution of the canopy elements in clumped canopies (Myineni et al., 1989)

$$\xi_{sl,i} = \Omega \exp[-K_b(\Psi) \Omega L_{t,i}], \quad (4)$$

where $L_{t,i} = \int_{z_i}^h \Lambda_{l,t}(z_i) dz$ is the total leaf area above layer i . The shaded leaves receive only diffuse radiation while the sunlit leaves are exposed also to direct sunlight. In this case, the amount of radiation absorbed per unit (un-clumped) leaf area (Wm^{-2} (leaf)) is obtained from the radiation profiles as

$$Q_{a,sh,i} = (1 - \alpha) K_d \Omega [Q_{d,i} + Q_{u,i}] \quad (5)$$

$$Q_{a,sl,i} = (1 - \alpha) K_b(\Psi) Q_{b,0} + Q_{a,sh,i},$$

where the extinction coefficients $K_b(\Psi)$ and K_d account for the mean leaf orientation with respect to direct beam and hemispherical radiation, and scaling the diffuse components by Ω is required for energy conservation (Eq. (3)). Computation of longwave radiation is simplified by neglecting multiple scattering and assuming the canopy elements are in thermodynamic equilibrium with ambient air, i.e. their T is equal to $T_a(z)$. In layer i , the net isothermal longwave radiation of a canopy element is $LW_i^* = LW_{d,i} + LW_{u,i} - 2\epsilon\sigma T_{a,i}$, where downward and upward components are

$$LW_{d,i} = \tau_{d,i} LW_{d,i-1} - (1 - \tau_{d,i})\epsilon\sigma T_{a,i-1} \quad (6)$$

$$LW_{u,i} = \tau_{d,i} LW_{u,i+1} - (1 - \tau_{d,i})\epsilon\sigma T_{a,i+1}.$$

At the canopy top $LW_{d,0} = \epsilon_{atm}\sigma T_a^4$ and the atmospheric emissivity ϵ_{atm} is estimated from measured T_a , vapor pressure e_a and cloudiness (Niemelä et al., 2001; Maykut and Church, 1973) (Suppl. 2). The lower boundary condition for LW_u is determined by the emissivity and temperature of the forest floor. The absorbed isothermal

net radiation (Leuning et al., 1995) used in the solution of the leaf energy balance (Eq. (16)) is $R_{n,i}^* = \sum Q_{a,i} + LW_i^*$, where $\sum Q_{a,i}$ includes both absorbed PAR and NIR.

2.1.2. Rainfall interception and throughfall

Rainfall interception and the wet leaf energy balance sub-model provide profiles of water storage per unit plant area $w(z)$ (kg m^{-2}), throughfall rate $P(z)$ ($\text{kg m}^{-2} \text{s}^{-1} = \text{mm s}^{-1}$) and evaporation/condensation rate $f_{e,w}(z)$ and sensible heat flux $f_{h,w}(z)$ from the wet plant parts. The multi-layer interception model is adopted from Watanabe and Mizutani (1996) and Tanaka (2002), and considers canopy elements as shallow tanks filled with intercepted precipitation and condensation, and depleted by evaporation and drainage of excess water. Canopy elements in a layer are considered either fully wet or fully dry, and intercepted precipitation can be retained only on dry fraction of plant area $df = 1 - w/w_{\max}$ (–), where $w_{\max}(z)$ (kg m^{-2}) is the water storage capacity per unit leaf area. Interception on wet fraction ($1-df$) of the canopy layer is instantaneously drained and contributes to $P(z)$.

When evaporation ($f_{e,w} > 0$) from wet fraction occurs, the change in $w(z)$ and $P(z)$ are (Watanabe and Mizutani, 1996)

$$\begin{aligned} \frac{\partial w}{\partial t} &= \left(1 - \frac{w}{w_{\max}}\right) P - \frac{w}{w_{\max}} f_{e,w} \\ \frac{\partial P}{\partial z} &= \Lambda_{l,t} \left(1 - \frac{w}{w_{\max}}\right) P, \end{aligned} \quad (7)$$

where precipitation is assumed to fall vertically. The water storage of a canopy layer is $W = w \Lambda_{l,t} \Delta z$ (kg m^{-2} (ground)), where Δz is a layer thickness and $\Lambda_{l,t} \Delta z$ the leaf area index ($\text{m}^2 \text{m}^{-2}$) in the layer. If condensation ($f_{e,w} < 0$) occurs within a canopy layer, Eq. (7) is modified to account for the additional moisture input as in Watanabe and Mizutani (1996).

2.1.3. Upscaling from leaf to canopy scale

In a planar homogenous canopy and in the absence of subsidence, the stationary mean continuity equation of a scalar s emitted or absorbed by the canopy reduces to (Juang et al., 2008)

$$\frac{\partial F_s}{\partial z} = \Sigma S_s(z), \quad (8)$$

where F_s is the total flux assumed to be primarily due to turbulence (i.e. ignoring molecular fluxes and stresses) and ΣS_s is sink/source density in a canopy layer. In APES, the scalar transfer is first solved per unit sunlit and shaded leaf area of each *PlantType* and canopy layer (Section 2.2), and then upscaled to provide $\Sigma S_s(z)$. Upscaling of heat (f_h), water vapor (f_e) and CO_2 (f_c) fluxes assumes that both dry and wet leaves can simultaneously co-exist in a canopy layer but transpiration and photosynthesis can occur only from the dry parts. The sink sink/source distributions of heat, water vapor and CO_2 of a single *PlantType* become

$$S_h(z) = \underbrace{\Lambda_l [f_{h,sl}\xi_{sl} + f_{h,sh}(1 - \xi_{sl})]}_{\text{dry leaves}} df + \underbrace{\Lambda_l f_h(1 - df)}_{\text{wet plant parts}} \quad (9)$$

$$S_e(z) = \Lambda_l [f_{e,sl}\xi_{sl} + f_{e,sh}(1 - \xi_{sl})] df + \Lambda_l f_{e,w}(1 - df), \quad (10)$$

$$S_c(z) = \Lambda_l [f_{c,sl}\xi_{sl} + f_{c,sh}(1 - \xi_{sl})] + \Lambda_w r_w, \quad (11)$$

where $r_w(z)$ ($\mu\text{mol m}^{-2} (\text{plant}) \text{s}^{-1}$) is the respiration rate of woody biomass. In case of condensation ($f_{e,w} < 0$) to a canopy layer, the term $(1 - df)$ is replaced by df in Eq. (10). The total $\Sigma S_s(z)$ is computed as the sum of contributions from all *PlantTypes* in a canopy layer.

Eq. (8) is solved using 1st-order turbulence closure (Suppl. 3), where the bottom layer and soil fluxes are included as boundary conditions and described in Sections 2.3 and 2.4. The stand scale

fluxes of sensible heat (H , W m^{-2}), water vapor (E , $\text{mmol m}^{-2} \text{s}^{-1}$) and CO_2 (F_c , $\mu\text{mol m}^{-2} \text{s}^{-1}$) are obtained by depth-integrating Eq. (8) over the canopy height.

2.2. Processes of vascular plants

2.2.1. Transfer of heat, H_2O and CO_2 between leaves and air

The air-leaf exchange of heat, H_2O and CO_2 are given by bulk (or path-length integrated) gradient-diffusion formulations (Eq. (1)) as

$$f_h = c_p g_{b,h} (T_l - T_a) \quad (12)$$

$$f_e = g_v^* (e_i - e_a) / p_a = g_v^* D_l / p_a \quad (13)$$

$$f_c = g_c^* (c_a - c_i), \quad (14)$$

where T_l is leaf temperature, $g_{b,h}$ leaf boundary layer conductance for heat ($\text{mol m}^{-2}(\text{leaf})$) and c_p is the specific heat heat capacity of air at constant pressure ($\text{J kg}^{-1} \text{K}^{-1}$); c_a and c_i (mol mol^{-1}) are ambient and internal CO_2 mixing ratios, respectively; e_a is ambient vapor pressure; $D_l = [e_s(T_l) - e_a]/p_a$ is the vapor pressure deficit at leaf temperature (mol mol^{-1}), where substomatal vapor pressure e_i is set at its saturation vapor pressure $e_s(T_l)$ determined by leaf temperature, and p_a is the atmospheric pressure (all in kPa). For low wind speeds occurring within a canopy layer, the effective conductances for CO_2 , g_c^* , and H_2O , g_v^* ($\text{mol m}^{-2}(\text{leaf}) \text{s}^{-1}$) include both stomatal g_s and leaf boundary layer $g_{b,i}$ conductances in series

$$g_c^* = \frac{g_{s,c} g_{b,c}}{g_{s,c} + g_{b,c}} \quad (15)$$

$$g_v^* = a_c g_c^*,$$

where $a_c \approx 1.6$ is the ratio of molecular diffusivity of H_2O to that of CO_2 in air. The $g_{b,i}$ are computed assuming leaves are flat plates and forced and free convection occur in parallel (Schuepp, 1993) (Suppl. 4), and g_s is linked with the economics of leaf gas exchange (Katul et al., 2010; Medlyn et al., 2012). In case of evaporation of intercepted precipitation or condensation of dew to leaf surfaces $g_v^* = g_{b,v}$.

Eqs. (12)–(15) are coupled through T_l necessitating an iterative solution to photosynthesis, stomatal conductance and leaf energy balance

$$\frac{\partial C_l T_l}{\partial t} = R_n - f_h - L f_e - \Sigma f_m, \quad (16)$$

where L is the latent heat of vaporization. Assuming the leaf heat capacity C_l and energy associated with metabolic processes Σf_m are negligible, linearising the net radiation as $R_n = R_n^* - c_p g_r (T_l - T_a)$, where $g_r = 4/c_p \epsilon_s \sigma T_d^3$ ($\text{mol m}^{-2} \text{s}^{-1}$) is the radiative conductance (Leuning et al., 1995), and substituting f_h and f_e from Eqs. (12) and (13), T_l can be solved as (Campbell and Norman, 1998)

$$T_l = T_a + \frac{R_n^* - L g_v^* D_l}{c_p (g_{b,h} + g_r)}. \quad (17)$$

2.2.2. Leaf photosynthesis, respiration and stomatal conductance

The biochemical demand for CO_2 at a leaf scale is described by the Farquhar model (Farquhar et al., 1980) giving f_c ($\mu\text{mol m}^{-2} \text{s}^{-1}$) as

$$f_c = \min[A_v, A_j] - r_d, \quad (18)$$

where A_v the Rubisco-limited and A_j the light-limited assimilation rate and r_d the leaf dark respiration rate. The potential sucrose transport limitation of photosynthesis (Campbell and Norman, 1998) are not considered but can be implemented if necessary. For the specific formulation of the model that of Medlyn et al. (2002) (Suppl. 5) is adopted. In the absence of water stress the maximum electron transport rate J_{max25} and dark respiration rate r_{d25} , at a reference temperature 25°C , are made linearly proportional

to maximum carboxylation rate (V_{cmax25} , Table 1) (Medlyn et al., 1999). Within a given *PlantType* V_{cmax25} varies with position in the canopy $f(z)$, seasonal cycle $f(S_d)$ (Suppl. 6) and pre-dawn leaf water potential $f(\psi_{pd})$ as

$$V_{cmax25} = V_{cmax25,ww} f(z) f(\psi_{pd}) f(S_d), \quad (19)$$

where $V_{cmax25,ww}$ is the value at the canopy top in well-watered conditions at 25°C . The $f(z)$ is proportional to vertical gradient of leaf nitrogen, described via attenuation coefficient k_N and cumulative leaf area L_t above z (Leuning et al., 1995; Kellomäki and Wang, 1997)

$$f(z) = \exp[-k_N L_t(z)]. \quad (20)$$

During drought-stressed periods, non-stomatal limitations of photosynthesis may occur via decreased mesophyll conductance or biochemical reductions related to decreasing Rubisco activity or electron transport capacity (Kellomäki and Wang, 1996; Keenan et al., 2010; Egea et al., 2011; Zhou et al., 2013). The biochemical limitations of V_{cmax25} and J_{max25} are accounted for as (Kellomäki and Wang, 1996)

$$f(\psi_{pd}) = \frac{1}{1 + (\psi_{pd}/\psi_0)^{\beta_0}}, \quad (21)$$

and that for r_{d25} as

$$f_{rd}(\psi_{pd}) = 1 + \left(\frac{\psi_{pd}}{\psi_0} \right)^{\beta_0}, \quad (22)$$

where pre-dawn leaf water potential ψ_{pd} is assumed hydrostatically connected to effective soil water potential in the root zone ψ_r (computed from Eq. (26)) as $\psi_{pd}(z) = \psi_r - z$ and ψ_0 and β_0 are empirical parameters.

Stomatal conductance g_s ($\text{mol m}^{-2} \text{s}^{-1}$) is based on a variant of the optimal stomatal control hypothesis (Katul et al., 2010; Medlyn et al., 2012). The 'unified stomatal model' is selected here due to frequent light limitations within the canopy, given for CO_2 as (Medlyn et al., 2012)

$$g_{s,c} = g_0 + \left(1 + \frac{g_1}{\sqrt{D_l}} \right) \frac{A_n}{c_s}, \quad (23)$$

where c_s is the CO_2 mixing ratio at leaf surface, g_0 ($\text{mol m}^{-2} \text{s}^{-1}$) is residual (cuticular) conductance and g_1 ($\text{kPa}^{0.5}$) an empirical parameter that is proportional to species-specific marginal water use efficiency $\lambda = \partial f_c / \partial f_e$ ($\text{mol}(\text{H}_2\text{O}) \text{mol}(\text{CO}_2)^{-1}$) as $g_1 \propto \sqrt{\Gamma_* / \lambda}$, where Γ_* is CO_2 compensation point. The value of λ in well-watered conditions and its (exponential) increase with decreasing ψ_{pd} during water stress have been shown to reflect plant water use strategies (Manzoni et al., 2010, 2013).

The functional dependency of g_1 on ψ_{pd} is given as (Zhou et al., 2013)

$$g_1(\psi_{pd}) = \min[0.2, g_{1,ww} \exp(\beta_1 \psi_{pd})], \quad (24)$$

where $g_{1,ww}$ refers to well-watered conditions, β_1 indicates the steepness of the decrease with increasing ψ_{pd} and g_1 is restricted to values above 0.2 to ensure numerical stability.

The woody biomass respiration r_w is computed as (Kolari et al., 2009)

$$r_w = R_{10} Q_{10}^{(T_a - 10)/10}, \quad (25)$$

where R_{10} is the base respiration rate ($\mu\text{mol m}^{-2}(\text{wood}) \text{s}^{-1}$) at 10°C , Q_{10} is the temperature sensitivity (–) and the wood temperature is approximated by T_a since the heat transfer within trunks are not explicitly considered.

2.2.3. Root water uptake

To couple leaf level processes and soil water dynamics (Eq. (32)), a recently proposed macroscopic root uptake model (Volpe et al., 2013), with some simplifying assumptions, is used to estimate water potential in root xylem ψ_r and root uptake profile R_i of each *PlantType*. When neglecting storage changes within the plant hydraulic system (roots, trunk, branches, and leaves), the plant transpiration rate T_r must be set to the total root-water uptake rate so that

$$T_r = \sum_i R_i = \sum_i g_{sr,i} (\psi_{s,i} - \psi_r), \quad (26)$$

where $\psi_{s,i}$ is the soil water potential in layer i , and ψ_r assumed uniform throughout the root system. The conductance $g_{sr,i}$ (s^{-1}) for water movement from bulk soil to root xylem is computed from the local soil hydraulic conductivity $K_{L,i}$, fine root area density $\Lambda_{r,i}$, characteristic fine root radius and root membrane conductivity as in Volpe et al. (2013). The ψ_r can be directly solved from Eq. (26) provided the T_r is known. When $T_r \simeq 0$ as in predawn, ψ_r gives ‘effective’ ψ_s sensed by the root system, which is here used to compute ψ_{pd} to model temporal variation of biochemical parameters (Eqs. (21)–(22)) and g_1 (Eq. (24)). For the soil model, Eq. (26) provides root water uptake profile that dynamically adjust to changes in ψ_s and K_L within the limits set by $\Lambda_r(z)$. When $T_r \simeq 0$ it also gives a simplified representation of hydraulic redistribution that was shown (Volpe et al., 2013) to be commensurate in magnitude with more detailed 2 or 3-D root models (Siqueira et al., 2008; Manoli et al., 2014).

2.3. Bottom layer processes

2.3.1. Bryophyte energy and H_2O exchange

Contrary to vascular plant species whose stomata effectively regulate the leaf-air exchange, the energy, H_2O and CO_2 exchange rate of mosses and lichens with the atmosphere subjected to given environmental conditions are passively controlled by their canopy structure and hydration status (Kellomäki and Hari, 1976; Oechel and Cleve, 1986; Williams and Flanagan, 1996, 1998; Lange et al., 2001; Rice et al., 2001; Rice and Schneider, 2004). In APES, the living parts of bryophytes are described as a *BottomLayer* object uniformly distributed along the forest floor. The dead moss parts are lumped within the soil profile.

The rate of change of bryophyte layer heat content ($W m^{-2}$) is

$$\frac{\partial C_m T_m}{\partial t} = R_n - H_m - LE_m - G_m + I_m, \quad (27)$$

where T_m is the bryophyte layer temperature, and the heat capacity C_m is computed as a sum of heat capacities of water and dry organic matter. Heat advection is $I_m = \rho_w c_w I_r T_p$, where ρ_w and T_p are density and temperature of intercepted precipitation I_r . Heat conduction between the living bryophytes and the topmost soil layer is

$$G_m = \lambda_h \frac{T_m - T_{s,1}}{\Delta z_m + \Delta z_{s1}}, \quad (28)$$

where Δz_m is the height of the bryophyte layer, Δz_{s1} and $T_{s,1}$ are depth and temperature of the topmost soil node, and the thermal conductivity λ_h ($W m^{-1} K^{-1}$) is calculated as the geometric mean (Ogée and Brunet, 2002). The λ_h of organic matter is a function of volumetric water content θ ($m^3 m^{-3}$) and given as $\lambda_h(\theta) = 0.03 + 0.5\theta$ (O'Donnell et al., 2009).

The sensible and latent heat fluxes are calculated as $H_m = c_p g_{bh,m} (T_m - T_a)$ and $LE_m = L g_{v,m}^* (e_s(T_m) - e_a)/p_a$, where $g_{bh,m}$ is bryophyte canopy boundary layer conductance for heat and $g_{v,m}^*$ the effective conductance for H_2O including both boundary layer

conductance $g_{bv,m}$ and transfer within the moss tissue. The $g_{bv,m}$ is based on a wind tunnel study by Rice et al. (2001)

$$g_{bv,m} = \frac{\rho_a 10^{-3.18} Re^{1.61} D_v S_{cv}^{0.33}}{l_m}, \quad (29)$$

where D_v ($m^2 s^{-1}$) is molecular diffusivity of water vapor in air; ρ_a molar density of air ($mol m^{-3}$) and Re and S_{cv} (–) Reynolds and Schmidt numbers for H_2O . The l_m (m) describes the characteristic height of moss surface roughness elements, typically order of 3–12 mm (Rice et al., 2001). The $g_{bh,m} \simeq 0.89 g_{bv,m}$ due to different molecular diffusivity of heat and H_2O . When the moss is wet and evaporation originates from the moss surfaces, $g_{v,m}^* = g_{bv,m}$. When drying progresses, the evaporation rate is reduced by the additional resistance related to water transfer in the moss tissues. In these conditions $g_{v,m}^* = g_{bv,m} \times \min(0.1285w_m - 0.1285, 1)$ based on *Sphagnum sp.* and *Pleurozium schreberi* gas-exchange data of Williams and Flanagan (1996) (Suppl. 7).

To describe the dynamics of moss water content w_m ($g g^{-1}$ (dry mass)), constrained between maximum $w_{m,max}$ and minimum $w_{m,min}$ water storage capacities, a water budget is added to supplement Eq. (27). The water pool is drained by evaporation and filled by interception and condensation, similar to the canopy layers, and by capillary rise from the soil computed as

$$I_c = K_{ms} \frac{\psi_m - \psi_{s,1}}{\Delta z_m + \Delta z_{s1}}, \quad (30)$$

where ψ_m (m) is the moss water potential and the hydraulic conductivity $K_{ms}(\theta)$ (ms^{-1}) taken as the geometric mean of conductivities of the living moss and topmost soil layer.

2.3.2. Moss CO_2 exchange

The net CO_2 exchange $A_{n,m}$ ($\mu mol m^{-2} s^{-1}$) of bryophytes is also controlled by tissue water content. At w_m above an optimum range $A_{n,m}$ can be CO_2 limited due to slow diffusion through the water films adjacent to moss surfaces while the rates of metabolic processes decrease in excessively dry conditions (Silvola, 1991; Williams and Flanagan, 1996; Lange et al., 2001). A simple multiplicative model for $A_{n,m}$ ($\mu mol m^{-2} s^{-1}$) incorporating the hydration limitation is

$$A_{n,m,i} = LAI_{m,i} \left[\frac{A_{max} Q_{p,i}}{b + Q_{p,i}} \right] f_1(w_*) f_2(T_m) - r_m f_3(w_m), \quad (31)$$

where the term in brackets provides photosynthesis in optimum hydration and temperature, the A_{max} is light saturated photosynthetic rate and b ($\mu mol m^{-2} s^{-1}$) the PAR intensity ($Q_{p,i}$) when $A_{n,b}$ equals half of the saturated rate. For computing $A_{n,m}$, the moss canopy is divided into layers i with $LAI_{m,i} \leq 0.5 m^2 m^{-2}$, and attenuation of Q_p is assumed exponential with an extinction coefficient $K_d = 0.8$ (resembling that of diffuse radiation). The moss respiration rate $r_m = R_{10,m} Q_{10,m}^{(T_m - 10)/10}$.

Function f_1 describes the dependency of assimilation rate relative to the hydration status $w_* = w_m/w_{m,max}$ (–) based on Williams and Flanagan (1996). The photosynthetic temperature response f_2 and moisture dependency of r_m (f_3) are adopted from Frolking et al. (1996) (Fig. S6). The seasonal cycle of photosynthetic parameters are neglected and all changes are taken instantaneous and reversible. These assumptions can be relaxed when appropriate data are available.

2.4. Soil processes

2.4.1. Soil water and heat flow

The *SoilProfile*-object describes water and heat balance in a variably saturated soil column. The soil moisture dynamics are computed by a 1-D Richard's equation (van Dam and Feddes, 2000)

$$\frac{\partial \theta(\psi_s)}{\partial t} = \frac{\partial}{\partial z_s} \left[K_L(\psi_s) \frac{\partial \psi_s}{\partial z_s} + (K_L + K_{L,m}) \right] - R(z) - D(z), \quad (32)$$

where $z_s < 0$ (m) is depth below the soil surface, K_L (m s^{-1}) is the liquid hydraulic conductivity of soil matrix and R and D (s^{-1}) are sink/source terms due to root uptake (Eq. (26)) and lateral subsurface flow, respectively.

The θ is linked to ψ_s via the soil water retention curve (van Genuchten, 1980; Schaap and van Genuchten, 2006)

$$\theta(\psi_s) = \theta_{res} + \frac{\theta_{sat} - \theta_{res}}{(1 + |\alpha + \psi_s|^n)^m}, \quad (33)$$

where the saturated θ_{sat} and residual θ_{res} water contents ($\text{m}^3 \text{m}^{-3}$) and empirical shape parameters α (m), n (–) and $m = 1 - 1/n$ depend on soil type.

The hydraulic conductivity is given as (Schaap and van Genuchten, 2006)

$$K_L(\theta) = K_{L,sat} S_e^{1/2} [1 - (1 - S_e^{1/m})^m]^2, \quad (34)$$

where $K_{L,sat}$ (ms^{-1}) is the saturated hydraulic conductivity and $S_e = (\theta - \theta_{res})/(\theta_{sat} - \theta_{res})$ the effective saturation (–). When a soil layer wetness is above field capacity, i.e. $\psi_s < -1$ m, an adjustment for gravity-driven preferential flow is added through a macro-pore conductivity $K_{L,m}$ that in full saturation is assumed to be an order of magnitude larger than $K_{L,sat}$, but then decreases linearly with ψ_s and reaches zero at field capacity.

The upper boundary condition of Eq. (32) is given as a balance between infiltration, soil evaporation E_s and capillary rise to living mosses. The E_s is controlled either by the ability of the soil matrix to conduct water to the surface (van Dam and Feddes, 2000), or by maximum achievable evaporation rate through the bryophyte layer (Suppl. 8). The numerical implementation of Eq. (32), as well as the formulation of boundary conditions, is based on a finite-difference scheme of van Dam and Feddes (2000).

The soil heat balance is calculated by the conservation of heat combined with Fourier's heat conduction (Hansson et al., 2004)

$$\frac{\partial C_p T_s}{\partial t} = \frac{\partial}{\partial z} \left[\lambda_h(\theta) \frac{\partial T_s}{\partial z} \right] + C_w \frac{\partial q_l T_s}{\partial z}, \quad (35)$$

where C_w is the volumetric heat capacity ($\text{MJ m}^{-3} \text{K}^{-1}$) of liquid water and C_p that of soil (Suppl. 9), $\lambda_h(z)$ is the heat conductivity in soil ($\text{W m}^{-1} \text{K}^{-1}$) and $q_l(z)$ is the liquid water flow (ms^{-1}) that is included only at the first (soil top) calculation node (infiltration and soil evaporation). The λ_h for the mineral soil layers is based on de Vries (1963) (Suppl. 9), and for the organic layers near the soil surface it is based on O'Donnell et al. (2009). The upper and lower boundary conditions for the soil system are flux-based and the former is given by the heat conduction between the soil surface and the moss layer (G_m), and Eq. (35) is solved by a finite-difference scheme.

2.4.2. Soil respiration

The soil respiration $R_{e,s}$ ($\mu\text{mol m}^{-2} \text{s}^{-1}$) is adopted from Pumpanen et al. (2003)

$$R_{e,s} = f(\theta) R_{10,s} Q_{10,s}^{(\bar{T}_s - 10)/10}, \quad (36)$$

where $R_{10,s}$ and $Q_{10,s}$ are the base rate and the temperature sensitivity, respectively and \bar{T}_s is the average T_s in top 0.2 m of the soil.

The impact of soil moisture is included through $f(\theta)$ (Skopp et al., 1990)

$$f(\theta) = \min [a\theta^d, b(\theta_{sat} - \theta)^g, 1], \quad (37)$$

where the first and second terms account for drought limitations and anoxia effects formed in extensively wet conditions, respectively. The empirical parameters $a = 3.83$, $b = 4.43$, $d = 1.25$ and $g = 0.854$ represent fine silty soil (Skopp et al., 1990).

3. Materials and methods

3.1. Measurement site

The APES was parametrized for a boreal coniferous forest using published parameter values, shoot gas exchange data and vegetation and soil characteristics measured at the Hyttiälä SMEAR II research station in Southern Finland ($61^{\circ}51' \text{N}$, $24^{\circ}17' \text{E}$, 181 m above sea level) (Hari and Kulmala, 2005). The site is located on an even-aged coniferous stand sown in 1962 on a shallow mineral soil. The overstory consists of Scots pine (*Pinus sylvestris*) mixed with some Norway spruces (*Picea abies*) and deciduous species. In 2005, the overstory canopy height h was ~ 15 m, hemisurface (half of the total) $LAI \sim 3 \text{ m}^2 \text{ m}^{-2}$, tree density 1400 ha^{-1} and mean diameter at breast height ~ 0.16 m. The understory vegetation consists of seedlings of Norway spruce, Silver birch and other deciduous species (mean height ~ 4 m, $LAI \sim 0.5 \text{ m}^2 \text{ m}^{-2}$). The forest floor is covered by a shallow dwarf shrub layer (mean height ~ 0.3 m, $LAI \sim 0.7 \text{ m}^2 \text{ m}^{-2}$) and a dense moss layer underneath ($LAI_m \sim 1.0 \text{ m}^2 \text{ m}^{-2}$) (Kolari et al., 2006; Kulmala et al., 2008). Complete description of the site and its measurements can be found elsewhere (Hari and Kulmala, 2005), and only details necessary for the model application are repeated.

The APES predictions are compared against measurements collected for two contrasting growing seasons (defined here as 1st May to 30th September). The growing season of 2005 was rather humid throughout, while 2006 was characterized by an intensive drought in late July and early August (Fig. S1) that lead to strong reductions in shoot- and stand level gas-exchange (Duursma et al., 2008; Launiainen, 2010), but not significant changes in LAI . The comprehensive long-term flux measurements at the SMEAR II site, and data from a field campaign in 2005 that considered forest floor fluxes and canopy turbulence (Launiainen et al., 2007; Kulmala et al., 2008), allow evaluating the APES model performance against independent datasets that represent spatial scales larger than those used in the model parametrization. Turbulent fluxes of sensible heat (H), latent heat (LE) and net ecosystem exchange (F_c) measured by eddy-covariance (EC) technique both above the canopy (at 23 m height above ground) and in the trunk-space (at 3.5 m) (Launiainen et al., 2005, 2007, 2013), chamber-based latent heat and CO_2 fluxes from the field layer (Kulmala et al., 2008) and ground heat flux G (Launiainen, 2010) are used to evaluate the modeled mass and energy fluxes.

The predictions of θ and T_s are compared against spatially averaged measurements from 5 soil pits (Ilvesniemi et al., 2010) and total water storage computed from measured θ . In this calculation, the irregular shape of catchment bedrock (and soil depth) were accounted for by weighting measured θ (adjusted by stone content) by the fraction of total soil volume in each horizon (Ilvesniemi et al., 2010). The predictions of the turbulence sub-model are compared against measured mean wind speed, CO_2 , H_2O and air temperature profiles, and within-canopy radiation against observed PAR and R_n at 1 m above the forest floor (Launiainen et al., 2007, 2011).

Table 1

PlantType parameters. For undergrowth trees and understory shrubs only values differing from those of Scots pine are given. Typical range found in literature is given in parenthesis.

Parameters	Value (range)	Explanation	Source
<i>Scots pine overstory</i>			
LAI_{max} ($\text{m}^2 \text{m}^{-2}$)	3.0	Maximum 1-sided leaf-area index	Biomass inventory
LAI_{min} ($\text{m}^2 \text{m}^{-2}$)	$0.8 \times LAI_{max}$	Minimum over-wintering LAI	Finér (1996)
WAI ($\text{m}^2 \text{m}^{-2}$)	$0.15 \times LAI_{max}$	Woody area index	Approximated
RAI ($\text{m}^2 \text{m}^{-2}$)	5.0	Fine root area index	Measured, Ilvesniemi and Liu (2001)
$V_{cmax25,ww}$ ($\mu\text{mol m}^{-2} \text{s}^{-1}$)	38 (35–50)	Maximum carboxylation velocity at 25°C in well-watered conditions	Wang et al. (1996)
$J_{max25,ww}$ ($\mu\text{mol m}^{-2} \text{s}^{-1}$)	$2.1 \times V_{cmax25,ww}$ (1.8–2.4)	Maximum electron transport rate at 25°C	Medlyn et al. (1999)
$r_{d25,ww}$ ($\mu\text{mol m}^{-2} \text{s}^{-1}$)	$0.023 \times V_{cmax25,ww}$ (0.02–0.05)	Leaf dark respiration rate at 25°C	Niinemets (2002)
k_N (-)	0.5	Canopy nitrogen attenuation coefficient	Kellomäki and Wang (1997)
γ (mol mol^{-1})	0.2 (0.3–0.4)	Parameter related to quantum efficiency	Kellomäki and Wang (1996), adjusted to account shoot geometry
θ (-)	0.7 (0.5–0.8)	Curvature parameter of Farquhar-model	Wang et al. (1996)
a_c (-)	1.6	Relative diffusivity of H_2O to CO_2	
ψ_0 (MPa)	-2.04; -1.56; -2.53	Scaling coefficients for V_{cmax25} , J_{max25} and r_{d25} ψ_{pd} -response	Kellomäki and Wang (1996)
β_0 (MPa)	2.78; 3.94; 6.07	As above	Kellomäki and Wang (1996)
$g_{1,ww}$ ($\text{kPa}^{0.5}$)	2.2	Stomatal model slope	Shoot chambers
β_1 (-)	0.7	well-watered conditions	Shoot chambers
g_0 ($\text{mol m}^{-2} \text{s}^{-1}$)	10^{-3}	Parameter for $g_1(\psi_{pd})$ -response	Shoot chambers
l (m)	2×10^{-2}	Residual conductance	Compromise of needle length and width
a, b (-)	0.4; 2.7	Characteristic leaf length scale	Fitted by matching measured and modeled $\Lambda_l(z)$
α_p (-)	0.12	Weibull-distribution parameters for $\Lambda_l(z)$	
α_n (-)	0.55	Shoot PAR albedo	Adjusted to match canopy albedo
ϵ_l (-)	0.98	Shoot NIR albedo	Adjusted to match canopy albedo
w_{max} (mm LAI^{-1})	0.15 (0.1–0.3)	Needle emissivity	Campbell and Norman (1998)
$R_{w,10}$ ($\mu\text{mol m}^{-2} \text{s}^{-1}$)	0.3	Leaf water storage capacity	Calibrated against throughfall measurements
$Q_{w,10}$ ($\mu\text{mol m}^{-2} \text{s}^{-1}$)	$1.9 \mu\text{mol m}^{-2} \text{s}^{-1}$	Wood respiration rate at 10°C	Kolari et al. (2009)
		Wood respiration temperature sensitivity	Kolari et al. (2009)
<i>Undergrowth trees</i>			
LAI_{max} ($\text{m}^2 \text{m}^{-2}$)	0.5 $\text{m}^2 \text{m}^{-2}$		Biomass inventory
RAI ($\text{m}^2 \text{m}^{-2}$)	1.6		
$V_{cmax25,ww}$ ($\mu\text{mol m}^{-2} \text{s}^{-1}$)	35 (30–50)		
k_N (-)	0.0		Not accounted
<i>Understory shrubs</i>			
LAI_{max} ($\text{m}^2 \text{m}^{-2}$)	0.7		Biomass inventory
LAI_{min} ($\text{m}^2 \text{m}^{-2}$)	$0.5 \times LAI_{max}$		
RAI ($\text{m}^2 \text{m}^{-2}$)	2.0		
$V_{cmax25,ww}$ ($\mu\text{mol m}^{-2} \text{s}^{-1}$)	20 (15–30)		Inferred from Gerdol et al. (2000)
r_{d25} ($\mu\text{mol m}^{-2} \text{s}^{-1}$)	$0.03 \times V_{cmax25}$ (0.02–0.08)		Inferred from Gerdol et al. (2000)
k_N (-)	0.0		Not accounted
$g_{1,ww}$ ($\text{kPa}^{0.5}$)	5		Inferred from Gerdol et al. (2000)
l (m)	1×10^{-2}		Leaf width
a, b (-)	4; 1		Approximated

3.2. Model parametrization

3.2.1. PlantTypes

To provide a simplified representation of the canopy composition, three *PlantTypes* were used – a pine overstory, spruce/birch undergrowth and Vaccinium-type shrubs (Table 1 and Fig. 1). To insure continuous and smooth leaf-area density Λ_l profiles, a two-parameter Weibull distribution function was employed (Teské and Thistle, 2004)

$$\Lambda_l(z_n) = -\frac{c}{b} \left(\frac{1-z_n}{b} \right)^{c-1} \frac{\exp[-((1-z_n)/b)^c]}{1-\exp[(-1/b)^c]} LAI, \quad (38)$$

where $z_n = z/h$ is normalized height, h (m) is mean canopy height and b and c are shape and scale parameters, respectively. For all species, the shape of woody area density (Λ_w) was assumed identical to Λ_l and set to 0.15 LAI . The root area densities as function of

soil depth z_s are described as $\Lambda_r(z_s) = -b^{z_s} \ln(b) RAI$, where parameter $b = 0.95$ is inferred from biomass measurements reported in Ilvesniemi and Liu (2001). In this study, they estimate total fine-root (diameter $\leq 2\text{mm}$) $RAI \sim 8.8 \text{ m}^2 \text{ m}^{-2}$, which was here partitioned between plant types as is their LAI and roots are assumed to exist in the whole mineral soil profile. Note that Λ_r acts here only as a scaling variable for computing root water uptake distribution and ψ_r and thus uncertainties in RAI are not crucial for the model behaviour.

For Scots pine overstory and undergrowth trees, the values of photosynthetic parameters in well-watered conditions, and their vertical gradient in the canopy were obtained from literature (Wang et al., 1996; Kellomäki and Wang, 1996) and re-scaled to represent values per hemisurface leaf area assuming the ratio between total and projected needle area is 2.8 (Niinemets and Kull, 1995). The biochemical limitations on V_{cmax25} , J_{max25} and r_{d25} due

Table 2
BottomLayer parameters.

Parameters	Value (range)	Explanation	Source
M_b (g m ⁻²)	60	Moss dry biomass	Measured, Kulmala et al. (2008)
LAI_m	1.0 m ² m ⁻²	Moss leaf-area index	Estimated from biomass and SLA
z_m (m)	0.05	Height of living mosses	Measured
l_m (m)	0.01	Characteristic roughness height of moss canopy	Estimate
$w_{m,\max}$ (g g ⁻¹)	10	Maximum water content (fresh/dry mass)	Williams and Flanagan (1996), Rice (2012)
$w_{m,\min}$ (g g ⁻¹)	1.5	Minimum water content (fresh/dry mass)	Williams and Flanagan (1996), Frolking et al. (1996)
$A_{m,\max}$ ($\mu\text{mol m}^{-2} \text{s}^{-1}$)	1.8	Maximum photosynthetic rate per unit leaf area	Kulmala et al. (2011), Williams and Flanagan (1998)
b ($\mu\text{mol m}^{-2} \text{s}^{-1}$)	50	Light half-saturation level	Kulmala et al. (2011)
$R_{m,10}$ ($\mu\text{mol m}^{-2} \text{s}^{-1}$)	0.2	Moss respiration rate at 10 °C	Williams and Flanagan (1998)
$Q_{m,10}$ ($\mu\text{mol m}^{-2} \text{s}^{-1}$)	2.0	Moss respiration temperature sensitivity	Williams and Flanagan (1998)
$\alpha_{p,m}$ (-)	0.05	Moss PAR albedo	Gaalen et al. (2007)
$\alpha_{n,m}$ (-)	0.45	Moss NIR albedo	Gaalen et al. (2007)
ϵ (-)	0.98	Moss emissivity	Campbell and Norman (1998)

decreasing water potential (Eqs. (21)–(22)) were adopted from shoot-scale measurements of [Kellomäki and Wang \(1996\)](#) in ambient CO₂ and temperature.

The stomatal model (Eq. (23)) slope $g_{1,ww}$ in well-watered conditions and its sensitivity to water potential (Eq. (24)) were inferred from shoot gas exchange data measured at the site during the 2006. To obtain g_0 and $g_{1,ww}$, the $g_{s,c}$ was computed from shoot chamber measurements and Eq. (23) was fitted to data over days 160–200, a period when full spring recovery had occurred but no signs of water stress were visible. Only data measured in dry-canopy daytime conditions ($Q_p \geq 100 \mu\text{mol m}^{-2} \text{s}^{-2}$ and $RH \leq 85\%$) were used. Second, the g_0 was set equal to the obtained value, treated as a constant, and the least squares fitting was repeated in three-day windows, with two day overlap, to resolve the temporal variability of g_1 . Finally, the $g_{1,ww}$ and β_1 were determined by non-linear least squares fit of Eq. (23) using derived g_1 as dependent and the measured soil water potential ψ_s in A-horizon (5–11 cm depth) as the independent variable. Only g_1 values from regressions whose coefficient of determination $R^2 \geq 0.4$ were used to ensure statistical significance. In the absence of data, drought responses and temperature sensitivity of V_{cmax} , J_{max} and r_d of all *PlantTypes* were assigned to those of Scots pine ([Wang et al., 1996; Kellomäki and Wang, 1996](#)).

The $V_{cmax25,ww}$ of *Vaccinium* shrubs was approximated indirectly by fitting the combined photosynthesis– g_s -model to gas-exchange measurements of *V. myrtillus* and *V. vitis-idaea* ([Lundell et al., 2008; Gerdol et al., 2000](#)) assuming leaf $c_i/c_a \sim 0.8$ and neglecting the effects of *T*. The $g_{1,ww}$ was then selected so that in light-saturated conditions, modeled water use efficiency (WUE) matches those reported by [Gerdol et al. \(2000\)](#). Other kinetic parameters of the Farquhar-model and their temperature sensitivity are taken as ‘generic’ ([Medlyn et al., 2002](#)). Woody biomass respiration was parametrized against trunk-chamber data from the SMEAR II ([Kolari et al., 2009](#)).

3.2.2. BottomLayer

Structural properties of the moss layer at the forest floor (Table 2) are based on average values within the sub-canopy EC footprint area ([Kulmala et al., 2008](#)). The photosynthetic parameters $A_{m,\max}$ and b are from field measurements of feather mosses *Pleurozium scheberi* and *Dicranum polysetum* ([Kulmala et al., 2011](#)) and moss dry biomass converted to LAI_m using specific leaf area of feather mosses ~ 160 –200 cm² g⁻¹ ([Bond-Lamberty and Gower, 2007](#)). In the absence of direct measurements from living mosses, their water retention curve and saturated hydraulic conductivity (Table 3) are approximated by those of fresh undecomposed boreal mor ([Laurén and Heiskanen, 1997](#)).

3.2.3. Stand microclimate

The stand leaf area index and its vertical distribution $\Lambda_{l,t}(z)$ is computed as the sum of all *PlantTypes*, and is used to model

vertical profiles of short- and long-wave radiation, turbulent transport as well as rainfall interception and canopy water budget (Fig. 1). The leaf angle distribution is assumed spherical and the combined leaf/shoot clumping factor $\Omega \sim 0.7$ is based on [Smolander and Stenberg \(1996\)](#). The water storage capacity per unit plant area, w_{max} , is set to 0.15 mm LAI⁻¹ by calibrating the modeled cumulative throughfall against the mean of seven throughfall gauges located ~ 1 m above the forest floor ([Ilvesniemi et al., 2010](#)). The above-ground computational domain extends from the ground to 23 m height and is divided into 200 equally spaced layers. For computation of BottomLayer processes, microclimatic variables were taken from the first layer above the ground (~ 0.2 m).

3.2.4. Soil properties

At SMEAR II, the surface shape of the bedrock at the hilltop forms two depressions with known borders. Based on total soil volumes and surface areas of the ‘micro-catchments’, the average soil depth is only ~ 0.6 m, and consists of a shallow organic horizon and a podsol profile formed on glacial till ([Ilvesniemi et al., 2010](#)). Hydraulic properties (Table 3) were determined by fitting Eq. (33) to water retention curves collected at the site ([Haataja and Vesala, 1997](#)). Following [Bouwer and Rice \(1984\)](#), the θ_{sat} and θ_{res} were adjusted by the volumetric fraction of stones ([Ilvesniemi et al., 2010](#)). Laboratory and field measured water retention curves differed markedly in the A-horizon, and therefore the water retention curve from B-horizon was used for whole 5–35 cm layer. For the organic layer consisting of poorly decomposed moss and litter on top of a humus layer, data from [Laurén and Heiskanen \(1997\)](#) were used.

The bedrock was assumed impermeable and lateral subsurface flow occurs only in the saturated part of the profile determined from $D(z) = K_{L,m}/\Delta z_s \partial z/\partial x$, where Δz_s (m) is the thickness of saturated layer(s) and hydraulic gradient $\partial z/\partial x \sim 0.04$ coincides with the average slope of the site. Other physical properties for estimating soil thermal characteristics (Suppl. 8) are derived from [Haataja and Vesala \(1997\)](#) and [Melkerud et al. \(2000\)](#). The soil domain was divided in 2 cm (1 cm near the surface) horizontal layers, and initial values of θ and T_s were set to their measured values. The heat conduction through the lower boundary ($i=N$) is computed as $G_N = \lambda_h \partial T_s / \partial z_s|_N$, where the gradient is obtained by solving Eq. (35) separately for the bedrock layer at each Δt using $T_{s,N}$ from previous Δt as the upper boundary condition. The bedrock was assumed homogeneous, $\lambda_h = 3.0 \text{ W m}^{-1} \text{ K}^{-1}$ equaling that of granite and T at 10 m depth equal to annual mean temperature (+4.5 °C). The initial T profile in the bedrock was calculated by forcing the heat equation with the measured C-horizon temperature for two years prior to commencement of the model runs so as to eliminate the effects of the initial conditions.

Table 3

Hydrologic properties of moss and soil layers. Moss and humus (H) layer parameters are based on Laurén and Heiskanen (1997) and A–C horizons on measurements from the site.

Horizon	Depth (cm)	θ_s ($\text{m}^3 \text{m}^{-3}$)	θ_r ($\text{m}^3 \text{m}^{-3}$)	$\alpha(\text{m})$	$n(-)$	K_{Lsat} (cm h^{-1})	Fract. of stones (-)
Living moss	+5–0	0.97	0.01	1.72	1.25	0.6	–
Dead moss	0–3	0.90	0.01	0.95	1.30	2.0	–
H	3–5	0.80	0.01	0.70	1.25	1.5	–
A	5–11	0.50	0.08	0.06	1.35	0.75	0.26
B	11–35	0.50	0.08	0.06	1.35	1.1	0.34
C	35–	0.41	0.03	0.05	1.21	1.5	0.44

4. Results and discussion

To address the study objectives, the performance of APES is first evaluated against measured energy, H_2O and CO_2 fluxes and environmental data in the moist 2005 growing season. This period was selected because soil water availability did not restrict gas exchange. Then, soil controls on the leaf and stand gas exchange and *BottomLayer* processes are discussed in the context of experiments in 2006. The meteorological conditions in 2005 and 2006 are shown in the Supplementary material (Fig. S1).

4.1. Radiation and scalar profiles in the canopy

Realistic description of the radiation regime is prerequisite for modeling leaf gas and energy exchange. Fig. 2 shows that when clear sky conditions prevail during nighttime, the model does not fully capture the negative radiation balance ($\sim 100 \text{ W m}^{-2}$, Fig. 2a) above the canopy, and marginally overestimates R_n also at the forest floor. However, the predictions agree well in cloudy conditions, which suggests that atmospheric emissivity and downwelling long-wave radiation $LW_{d,0}$ are overestimated in clear-sky conditions. Note that in the absence of direct measurements of $LW_{d,0}$, e_{atm} was estimated from near-surface T_a , vapor pressure and cloud-cover fraction retrospectively – and all determined from surface observations (Suppl. 2).

To reproduce the measured canopy albedos and R_n (Fig. 2), it was found necessary to reduce α (Table 1) from its measured leaf/needle single-scattering albedo (~ 0.15 and ~ 0.7 for PAR and NIR, respectively). The magnitude of the adjustment here is similar to Ni-Meister et al. (2010). In this aforementioned study, a single coniferous shoot was proposed as the basic scattering element (see Section 2.1.1) instead of a single needle. Further, the sensitivity analysis indicated that such an increase in absorbed shortwave radiation leads to larger sensible heat flux from the over-story canopy, while stand latent heat flux and CO_2 exchange are only marginally affected (not shown). After this adjustment, the radiation sub-model captures the diurnal and seasonal variability of mean R_n and PAR above the forest floor, although spatial variability is significant especially on cloudless days (Fig. 2).

The comparison of modeled and measured ensemble averaged profiles of wind speed, air temperature and CO_2 and H_2O mixing ratios in daytime and nighttime (Fig. S3) indicate that APES with the 1st-order turbulence closure scheme can resolve most of the vertical variability of within-canopy scalar gradients despite the well-known limitations of such gradient-diffusion closure.

4.2. CO_2 , H_2O and heat fluxes

Figs. 3 and 4 show a comparison between modeled and EC-measured 1/2 h CO_2 and latent heat fluxes in 2005. At the stand scale, both diurnal and seasonal cycles of $F_{c,a}$ are well reproduced (Fig. 3). In an ensemble sense, the variability of $F_{c,a}$ is well captured and the scatter remains small, especially when considering the dynamic footprint and random variability of measured turbulent fluxes (Aubinet et al., 2012). The temporal biases result mostly

from errors in the respiration components. This finding is particularly true for the R_s since the current model version does not consider linkages between plant carbon uptake and root respiration, or temporal variability of microbial activity (beyond T_s and θ), i.e. changes in $R_{s,10}$ over the growing season (Kolari et al., 2009). The seasonal and diurnal variability of LE_a , i.e. stand evapotranspiration, is also well predicted (Fig. 4). In 2006, the linear regression between modeled (y) and measured (x) fluxes was $y = 0.98x - 0.89$ ($R^2 = 0.73$) for $F_{c,a}$ and $y = 0.83x + 15$ ($R^2 = 0.72$) for LE_a ; the marginally poorer correspondence is mainly due to errors during the drought-stress discussed later. In transitional periods such as those in the morning and in the evening, the measured fluxes are small and the model overestimates LE_a by $\sim 10 \text{ W m}^{-2}$ compared to measurements. It is to be noted that those conditions deviate appreciably from the assumed stationarity in the model development. Together with somewhat higher predicted than observed evaporation rates from the wet canopy state, the two results lead to a small positive bias reflected by the regression slope ≤ 1 used to evaluate the model performance (Fig. 4). The model yields an overestimation of cumulative LE_a from 10% (in 2006) to 15% (in 2005). Accounting for the spring recovery of photosynthetic capacity and seasonal development of LAI (Suppl. 6) was necessary for capturing the early growing season fluxes. When these dynamic factors were omitted and photosynthetic parameters assigned to their maximum summertime values throughout the growing season, over-estimation of the fluxes occurred in early to mid-May. This finding is also consistent with another study on a pine forest that showed how ignoring the dynamic variations of V_{cmax} along with LAI can lead to significant biases in above-canopy fluxes (Juang et al., 2008).

The sub-canopy EC measurements represent net exchange between the atmosphere and soil, understory, and undergrowth trees all lumped together. As expected, the scatter between modeled and measured LE_s is larger than above the canopy but the temporal variability and magnitude are reasonably captured (Fig. 4). Sensitivity analysis indicated that to reproduce measured LE_s , the WUE of understory shrubs/grasses should be lower than that of the Scots pine assuming that the micro-climate close the forest floor (Fig. 2 and Fig. S3) and total LAI of the understory shrubs are correctly estimated. This is supported by gas-exchange data of *Vaccinium myrtillus* and *Vaccinium vitis-idaea* (Gerdol et al., 2000) showing that $g_{1,ww} \sim 5–6$ (more than twice that of Scots pine) is representative. It may be conjectured that the much shorter hydraulic pathway of understory shrubs leads to water costs (in carbon units) that are smaller than those associated with the main Scots pine canopy, where the hydraulic pathway can be quite extensive.

The accuracy of EC-measured $F_{c,s}$ at the SMEAR II is compromised during nighttime periods due to low turbulence levels typically prevailing in the trunk-space. Consequently, the diurnal variability of $F_{c,s}$ cannot be reliably determined by the sub-canopy EC data (Launiainen et al., 2005; Kulmala et al., 2008). Fig. 3 and 4 also show forest floor fluxes measured by a transparent chamber (surface area $\sim 1 \text{ m}^2$) at three locations. During the first period, the forest floor vegetation in the chamber was similar on average to the vegetation within the footprint of the EC systems. The contribution of lingonberry and mosses were significantly higher in the

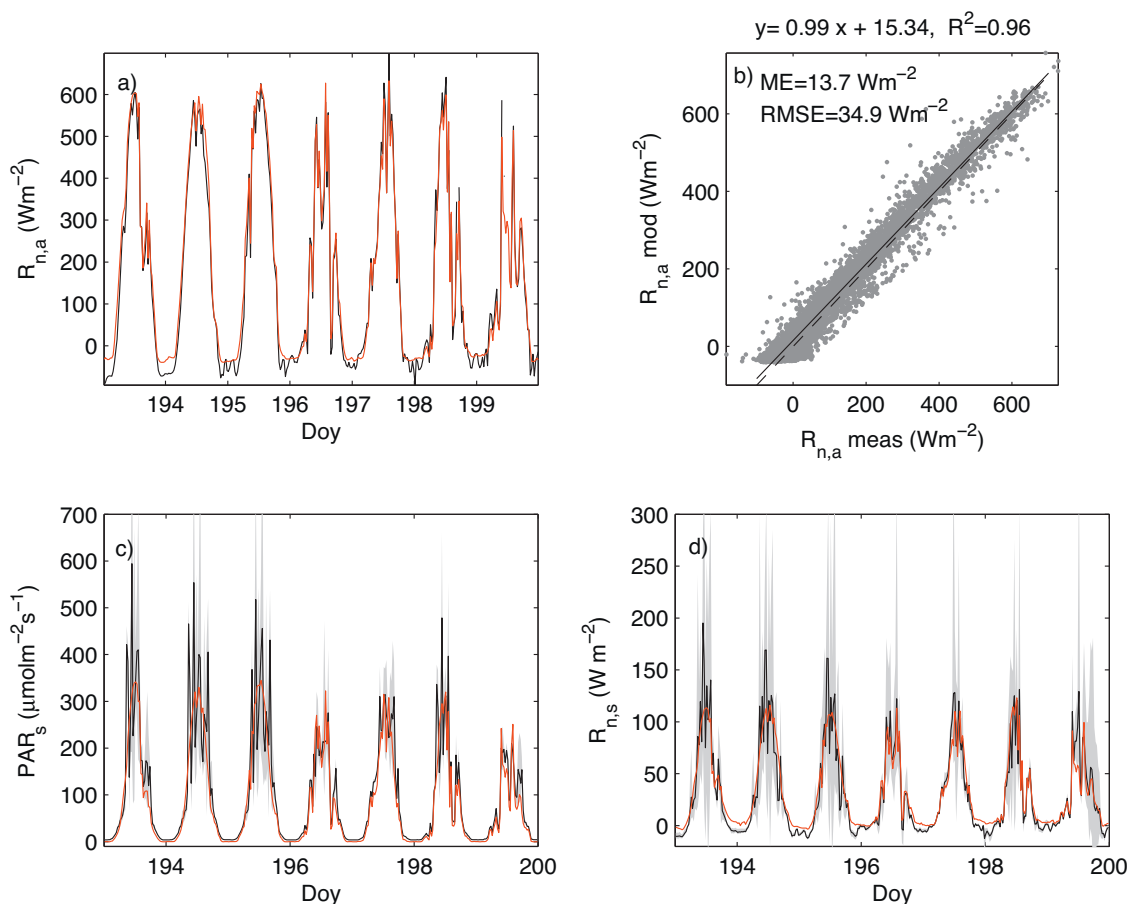


Fig. 2. Comparison of measured and modeled 1/2 net radiation $R_{n,a}$ above the canopy (a,b), and PAR_s (c) and (d) net radiation $R_{n,s}$, above the forest floor. Red line is model prediction and black line/grey range give mean and variability range of five radiation sensors. (For interpretation of the references to colour in this figure legend, the reader is referred to the web version of this article.)

latter locations (Kulmala et al., 2008). The chamber measurements represent the total flux from the soil, moss layer and understory shrubs, and their diurnal cycle is well captured by the model. The chamber fluxes showed higher soil respiration rates than predicted by the model – or captured by above-canopy EC measurements. Nevertheless, the APES predictions on sub-canopy CO₂ and latent heat exchange seem realistic and agree with independently measured fluxes, which increases the confidence in the model's ability to predict forest floor processes (recall those measurements were not used in any prior model calibration).

At the stand scale, the variability of modeled sensible heat flux H_a is higher than measured (Fig. 5). This is expected since the model conserves the energy while a ~10% energy balance closure gap is typical during the growing season at the SMEAR II-site (Launiainen, 2010). The sub-canopy sensible heat flux (H_s) is also well captured (along with a negligible bias), which suggests that part of LE_s bias when measured fluxes are low may be related to problems in EC measurements due to large relative humidity common within transitional periods (Mammarella et al., 2009). Layer-averaged leaf-air temperature difference ΔT (Fig. S3) is typically around +2.0 °C in the upper canopy during clear days, and never exceeded +4 °C (not shown). In the lower canopy, the majority of the foliage is in a shaded environment and layer-averaged ΔT remains below +1.0 °C. Due to the simplified assumption that leaves are either exposed to full sunlight or full shade (and leaf fluttering neglected), the part of the foliage assumed to be exposed to direct sunlight can become unrealistically warm ($\Delta T \sim +8$ °C) in the lower canopy where wind speeds are appreciably low. No direct measurements of canopy temperature were made but ΔT is in line with those reported for

coniferous species (Zha et al., 2013; Smith and Carter, 1988; Martin et al., 1999).

Fig. 5 shows that the model also reasonably captures the measured ground heat flux G in the A-horizon (~5–11 cm depth), which suggests that near-surface radiation environment, forest floor energy balance and thermal conductivity between the bryophyte layer and soil are realistic. The measured G shows some systematic difference among the three locations reflecting spatial variability in canopy closure, forest floor vegetation, micro-topography and soil structure.

4.3. Coupling above- and below-ground processes

4.3.1. Soil temperature and water balance

As typical for forest soils, the measured soil temperature (T_s) and volumetric water content exhibit large spatial variation in each horizon (Fig. 6) making direct evaluation of the model performance against point measurements infeasible. However, a number of observations can still be made: The soil profile rapidly warms in May and June, and modeled temperature in the A and B – horizons tend to become 1.0–3.0 °C warmer than measured. The diurnal amplitude and phase are correctly predicted at all depths suggesting that the heat diffusivity is reasonably modeled. In the organic layer and near the soil surface, the model captures the seasonal course and predicts diurnal amplitude and level of T_s to within 1.0–1.5 °C. Near the surface, soil heat flux and temperature are tightly coupled to the surface energy balance and thus larger amplitudes occur during clear days. Since the soil domain is shallow (only 0.6 m), T_s is sensitive to the assumed lower boundary

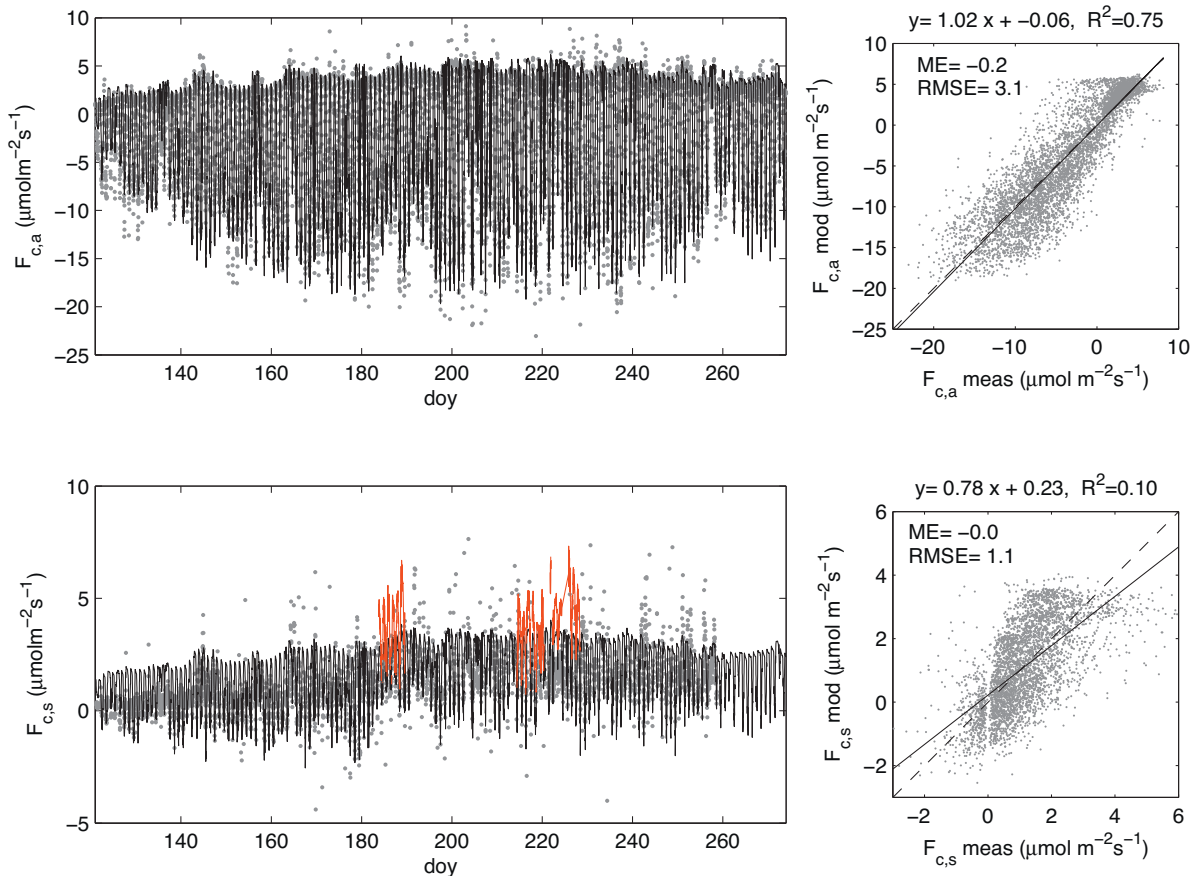


Fig. 3. Measured (gray) and modeled 1/2 h ecosystem CO₂ flux ($F_{c,a}$), representing net ecosystem exchange, and in sub-canopy ($F_{c,s}$), giving the net exchange between the forest floor, understory and the atmosphere. Scatterplots include linear least-squares regressions (solid line) and 1:1 lines (dashed). Also chamber-measured forest floor fluxes are included for three periods in 2005 (in red, see text). (For interpretation of the references to colour in this figure legend, the reader is referred to the web version of this article.)

condition formulated here liberally by heat conduction between the mineral soil profile and the bedrock instead of forcing a boundary soil temperature to a measured value.

The measured water content (θ) profile indicates rapid redistribution of water in the soil during and after infiltration events, which is not completely captured by the model. This model limitation becomes more pronounced in dry soils (as in 2006, not shown) where the hydraulic conductivity drop with ψ_s (Eq. (34)) and restricts rapid movement of water into the soil matrix. Thus, a dual-porosity approach is needed for a more realistic description of preferential flow and resulting soil water dynamics in forest soils (Beven and Germann, 1982). However, the total soil water storage is reasonably predicted and remains within 20 mm (or $\leq 15\%$) of the measured value throughout the wet growing season of 2005 while the correspondence is even better in the dry 2006 (Fig. 7). Note that such a 20 mm uncertainty in water storage within a 0.6 m deep soil profile corresponds to $<0.04 \text{ m}^3 \text{ m}^{-3}$ error in average volumetric water content.

The 2005 was characterized by several high-intensity rainfall events and the relative throughfall was higher than typical at the site (Ilvesniemi et al., 2010). Based on measurements, the over-story and undergrowth trees intercepted on average $\sim 14\text{--}16\%$ (50–55 mm) of the precipitation but the spatial variability was large reflecting the spatial inhomogeneity of stand closure. In forest gaps, the throughfall was similar to P above the main canopy. Below denser crowns, a maximum of 25% (90 mm) of the accumulated P (355 mm, 1st May–30th September 2005) was intercepted (not

shown). To match the measured average throughfall, the interception capacity in APES was set to $w_{\max} = 0.15 \text{ mm LAI}^{-1}$, which is in the lower range of values reported for coniferous species (Watanabe and Mizutani, 1996; Liu, 1998; Keim et al., 2006). This may be due to the canopy water budget sub-model that enables evaporation/condensation during and between rainfall episodes, while the measured interception capacities are often derived from measurements of “bulk” throughfall over a single or several rainfall events. Also, the mass and energy transport between wet plant elements and air are solely controlled by boundary layer conductance ($g_{b,v}$ and $g_{b,h}$) and thus the ‘optimal’ value of w_{\max} provides a best fit between measured and modeled interception rate depending on the selected characteristic leaf/shoot dimension l and mean velocity profile $U(z)$. Somewhat too strong evaporation rate during the wet canopy state (Fig. 4) here suggests that l used here may be small for predicting evaporation process from the wet surfaces. This can be due to the significance of branches and trunks acting as rainfall-intercepting media in coniferous species (Keim et al., 2006).

The predicted partitioning of stand water budget in the wet 2005 growing season are as follows: In total 62 mm (18% of P) is intercepted, and subsequently evaporated from the Scots pine overstory and undergrowth trees (55 mm) and understory shrubs (7 mm). In addition, mosses intercepted 14 mm (4% of P) and thus 280 mm (79%) infiltrated into the soil profile. Total stand transpiration was 211 mm, 71% of total stand evapotranspiration (ET, 298 mm). Transpiration was partitioned between the Scots pine overstory (167 mm or 79%), undergrowth trees (15 mm or 7%) and

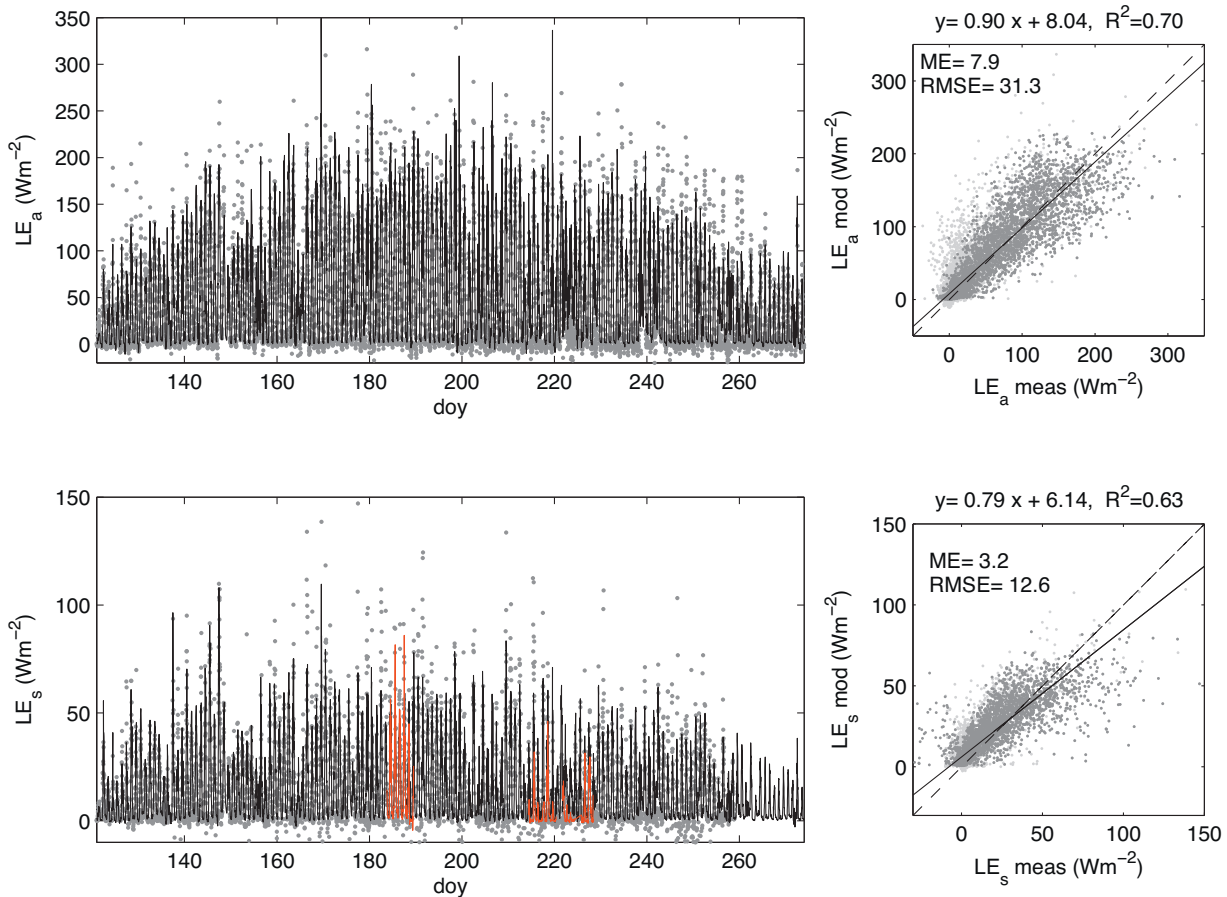


Fig. 4. As Fig. 3 but for latent heat flux LE . In scatterplots light grey dots show wet-canopy conditions.

understory shrubs (19 mm or 14%). Moss evaporation accounted for 17 mm (6% of ET), of which ~4 mm was capillary rise from the underlying organic layer, and direct evaporation from the soil was 9 mm (3%). During the wet growing season ca. 61 mm outflow occurred from the soil profile as subsurface runoff. The timing of runoff events matched the measured within 2 days (not shown) but comparison of total runoff was not possible due gaps in the data. In the dry 2006 growing season, P was markedly lower (208 mm) but stand ET (308 mm) and its partitioning were nearly similar to 2005 leading to stronger depletion of the soil water storage and concurrent decrease in soil water potential (Fig. 7).

4.3.2. Gas exchange during drought

Depletion of soil water resources in mid-July and August 2006 (Fig. 7) had significant feedback to Scots pine eco-physiology. Fig. 8 shows expected decreases of the stomatal model slope g_1 during drought stress. The coherent response to reduced soil water potential ψ_s suggest that despite the scatter, an exponential decrease in g_1 with ψ_s (Eq. (24)) proposed by a revised optimality theory (Manzoni et al., 2010, 2013) appears reasonable.

To explore how well the stand-scale CO_2 and H_2O exchange can be predicted during drought, three simulation runs are summarized in (Fig. 9). The first is a full APES simulation, which includes both biochemical (Eqs. (21)–(22)) and stomatal (Eq. (24)) limitations and computes ψ_{pd} from modeled root water potential ψ_r (Eq. (26)). To avoid errors in ψ_{pd} due to uncertainties related to biased root density profile, soil water retention characteristics and hydraulic conductivity – or accumulated errors in soil water balance, the second run uses measured soil water potential ψ_s in the A-horizon instead of ψ_r to estimate ψ_{pd} . The third run provides a

baseline when no feedbacks between leaf gas exchange and soil water availability are considered.

Fig. 9 shows that APES captures the general trend of decreasing stand CO_2 and latent heat fluxes (and subsequent increase of sensible heat flux, not shown) during the progressive drought as well as the recovery after ~10 mm precipitation event on day 229. However, during intense drought stress the diurnal cycles are not perfectly predicted, likely due to assuming ψ_l hydrostatically related to ψ_r and neglecting its diurnal variation. These simplifying assumptions can be relaxed by including a dynamic model of soil-xylem-leaf water transport (Hölttä et al., 2009; Chuang et al., 2006) and near-instantaneous linkage between ψ_l and leaf gas-exchange parameters. The results here propose that during moderate drought stress, stomatal limitations are stronger and more significant than adjustments in photosynthetic capacity. The latter becomes important only in more severe drought; the stomatal limitations alone were not sufficient to describe photosynthesis during days 223–229 when ψ_s dropped below -1.1 MPa and measured $F_{c,a}$ was less than half of its pre-drought level.

In dry soils, small uncertainties in water content can lead to order of magnitude error in water potential and hydraulic conductivity due the nonlinearities of the soil water retention curve (Eq. (33)) making the root water uptake distribution and predicted ψ_r sensitive to uncertainties in soil hydraulic characteristics (not shown). These uncertainties in ψ_s can become potentially severe when modeling stand latent heat exchange and energy partitioning (due to direct dependency on stomatal conductance) while $F_{c,a}$ appears less sensitive and is only affected in the driest conditions (due to the adjustment in c_i).

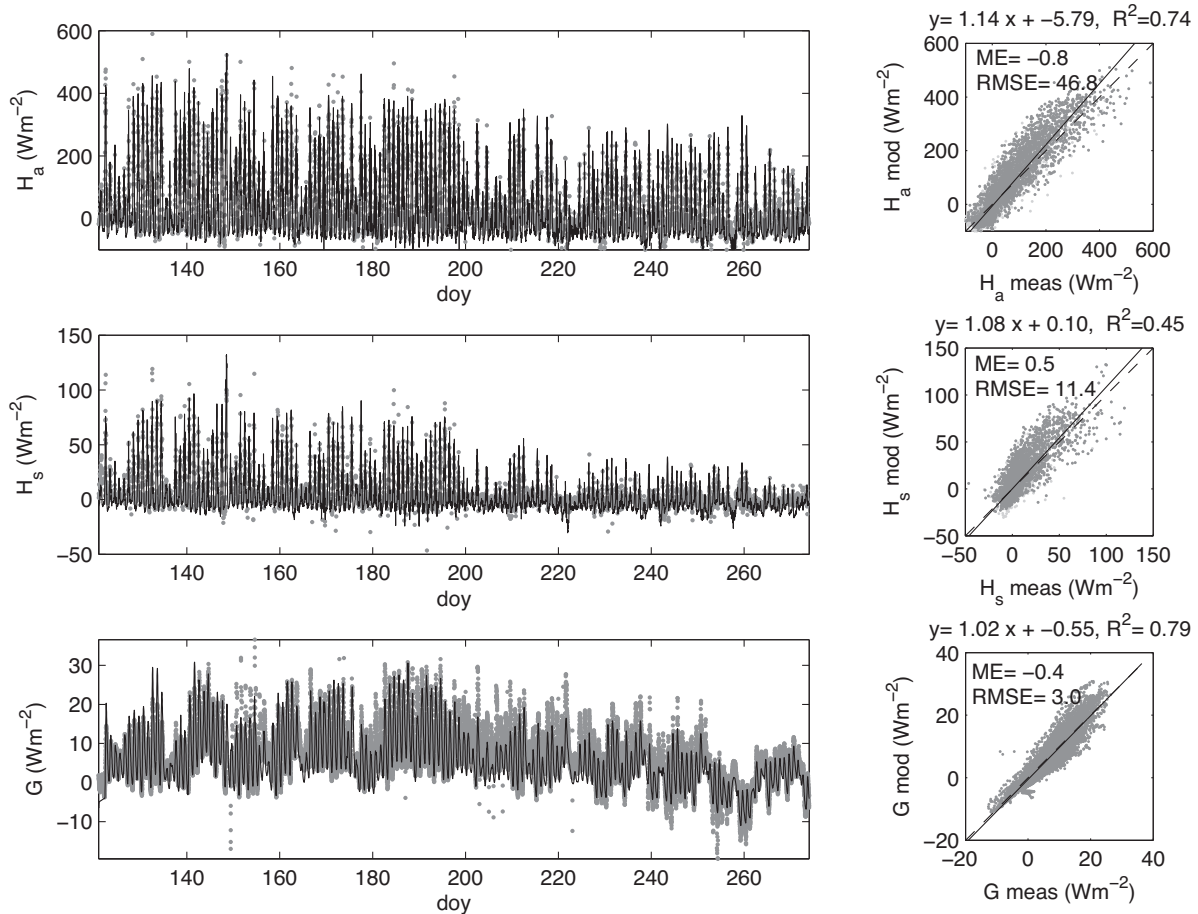


Fig. 5. Measured (gray) and modeled 1/2 h sensible heat fluxes at ecosystem scale (H_a) and in the sub-canopy (H_s). The predicted mean 1/2 h soil heat flux G at depth 10–15 cm is compared against measurements from three heat flux plates at similar depth (bottom). In the scatterplot of G , the model results are compared against average of the flux plates.

4.3.3. Moss moisture dynamics and fluxes

Finally, the hydraulic connection between the bryophyte layer and the soil water and its implications to CO_2 and energy exchanges are discussed. Assuming the living part of mosses can hold up to $\sim 10 \text{ g H}_2\text{O g}^{-1}$ (dry mass), the total storage capacity of *Bottom-Layer* at the SMEAR II site is on the order of $M_b w_{m,\max} \simeq 0.6 \text{ kg m}^{-2}$ (or mm). Thus in 2005, throughfall below the understory often lead to full saturation of moss tissues (Fig. 10). After precipitation, the water storage w_* decreases rapidly by evaporation, which is initially controlled by the ambient micro-climate and bryophyte structure. As drying progresses, the moss evaporation rate decreases due to the additional resistance for transporting water from tissues to the moss surface (Suppl. 7). With independently derived *BottomLayer* parameters, the predicted level and dynamics of measured moss water content is reasonably captured. The measured water contents are based on weighting several moss populations at few day intervals over the summer and autumn 2005.

Depending on the water potential gradient between the living mosses and the organic layer beneath, capillary rise is initiated in the drying mosses (Eq. (30)). The model suggests that when the organic layer is sufficiently moist, daily evaporation from the moss canopy can be compensated for by capillary rise. In conditions when the evaporative demand is high and precipitation infrequent, the hydraulic connection between the living moss and the organic soil layer is suppressed due rapidly decreasing hydraulic conductivity in the drying organic layer. During these periods, evaporation, photosynthesis and respiration are reduced

due the low w_* (Fig. 11). In very dry conditions, such as during the 2006 drought, soil evaporation (from beneath the mosses) switches from micro-climate controlled to soil-controlled and is significantly reduced (not shown). The literature on the role of capillary interaction on moss water budget is inconclusive (Carleton and Dunham, 1996; Rice, 2012; McCarter and Price, 2014). The model analysis here suggests that if the underlying soil is sufficiently moist, the capillary interaction can be an important mechanism allowing CO_2 assimilation between rainfall episodes. Sensitivity analysis also showed that when the moss saturated hydraulic conductivity was increased by an order of magnitude, predicted w_* remained constantly above 0.5 during the wet 2005 growing season suggesting that that approximation for moss hydraulic conductivity is reasonable although the exact value is uncertain.

The model results on the bryophyte energy balance (Fig. 11) propose that evaporation and heat conduction are the main modes of energy transfer (along LW) while sensible heat flux H_m remains small due to the low wind speed near the forest floor. This was the case even when adjustment to moss boundary layer conductance due free convection following Daamen and Simmonds (1996) was included. Sensitivity analysis indicated that sensible heat becomes a significant component of the moss energy balance in sparser stands where lower overstory and understory LAI allow higher radiation levels and more efficient turbulent exchange (canopy more ventilated) to occur from the moss layer. These physical factors are the main reason for higher LE_m and H_m rates in May (Fig. 11) when the total stand LAI was ~ 3.2 compared to $\sim 4.2 \text{ m}^2 \text{ m}^{-2}$ in September. The model predicts that when mosses are dry, their

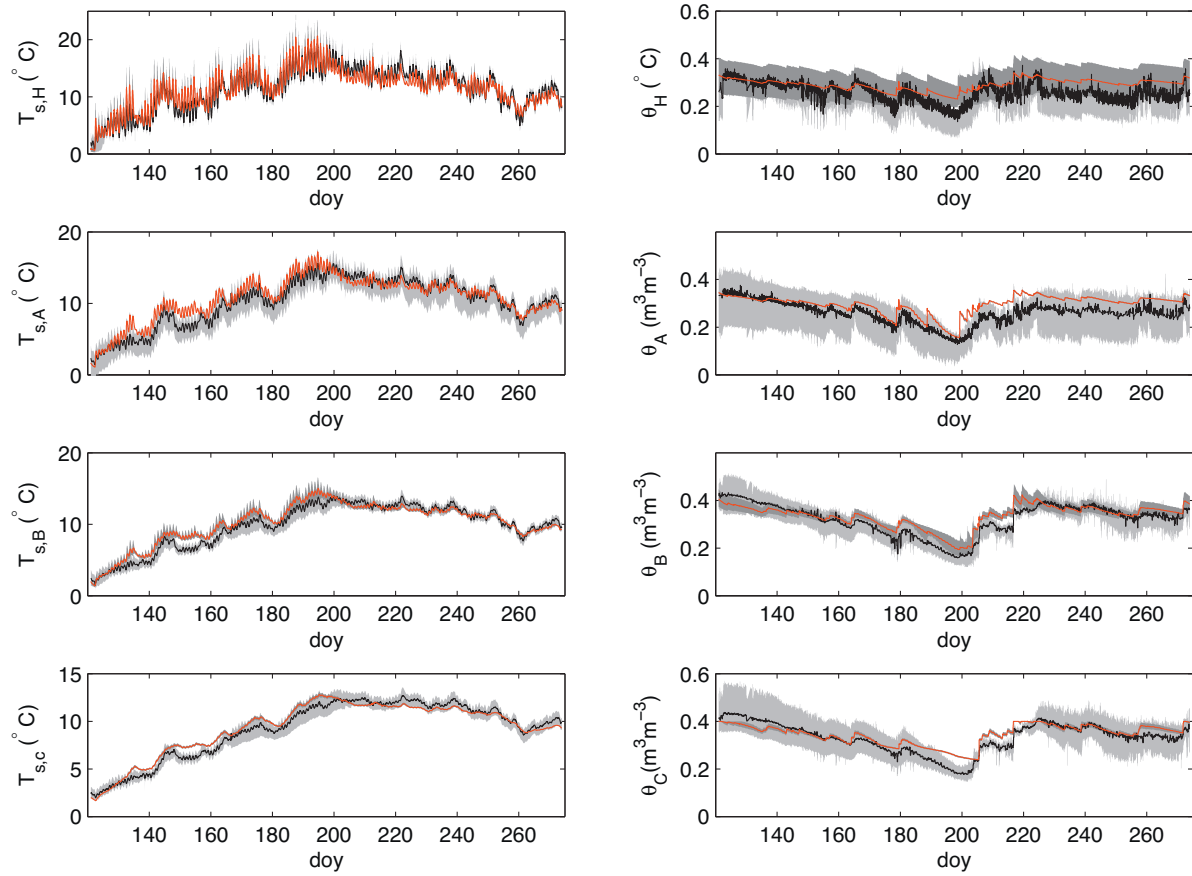


Fig. 6. Soil temperature T_s (left) and volumetric moisture content θ (right) in different soil horizons during 2005. The light gray area and black line indicate variability range and mean of the point measurements in a given soil layer, and the red line and the dark gray area represent the modeled mean and variability at similar depth. (For interpretation of the references to colour in this figure legend, the reader is referred to the web version of this article.)

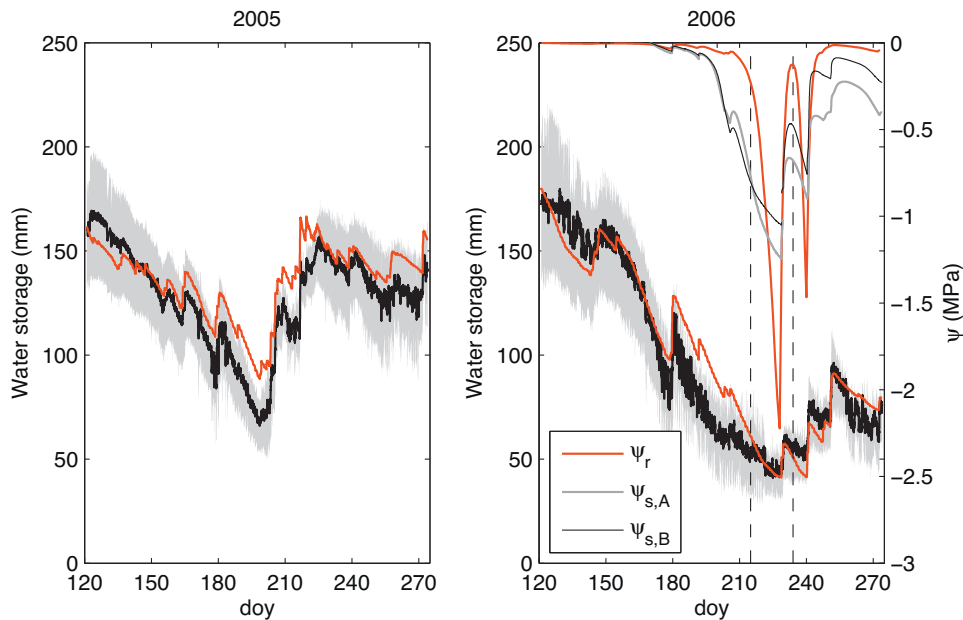


Fig. 7. Total water storage in the 0.6 m deep mineral soil profile in 2005 (a wet growing season) and in 2006 (a dry growing season). The black line and shaded grey area represent mean \pm one standard deviation and red line gives model prediction. Measured soil water potentials ψ_s in A and B horizons and computed root water potential ψ_r are shown during 2006. The dashed lines indicate the drought period shown in Fig. 9. (For interpretation of the references to colour in this figure legend, the reader is referred to the web version of this article.)

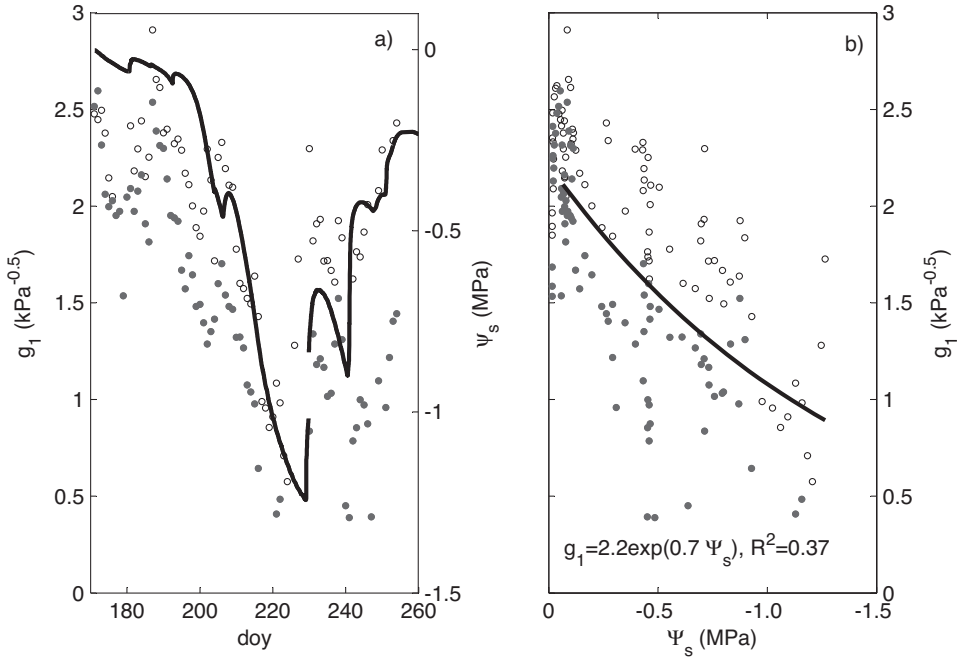


Fig. 8. Response of stomatal model slope g_1 (Eq. (23)) to measured A-horizon water potential Ψ_s . The (a) shows dynamics of g_1 and Ψ_s during 2006 drought and (b) gives the fit of Eq. (24). The circles show daily average g_1 derived from two shoot-chambers, and Eq. (24) is fitted to combined dataset.

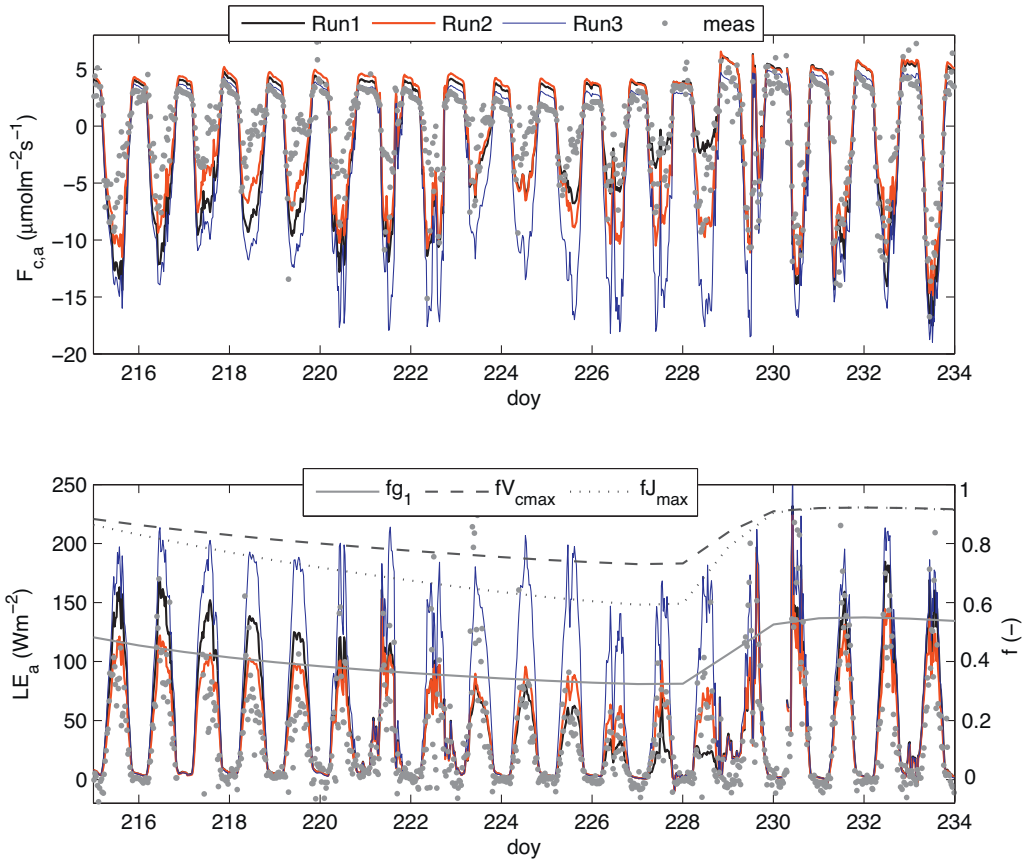


Fig. 9. Stand-scale CO₂ (F_{ca}) and latent heat (LE_a) fluxes during 2006 drought. Run1: fully coupled simulation where modeled root water potential is used to compute leaf water potential ψ_l used to adjust leaf-scale stomatal and biochemical parameters. Run 2: as Run 1 but using ψ_l derived from measured soil water potential (see text); Run 3: baseline when all feedbacks between ψ_l and leaf physiology are neglected. The magnitude of stomatal (fg_1) and biochemical adjustments (fV_{cmax} and fJ_{max}) in Run 2 are also shown.

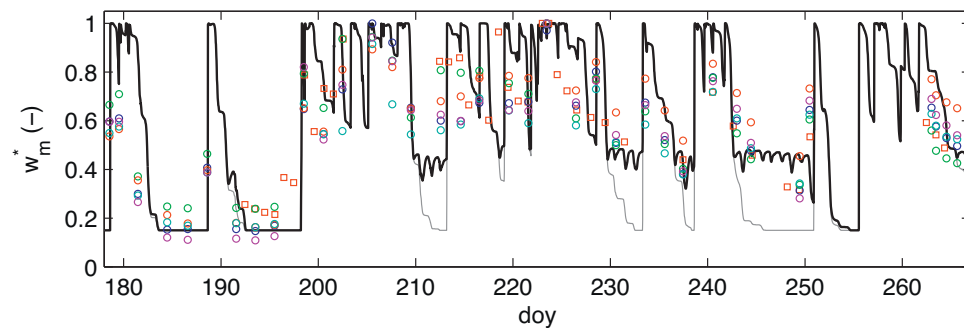


Fig. 10. Relative water content w^* (—) of the living moss layer in July–September 2005 with capillary rise enabled (thick line) and disabled (thin line). The symbols show measured water contents of different moss canopies.

temperature in this particular stand can rise to some 8–10 °C above local air temperature whereas nearly saturated mosses remain within 1–2 °C of T_a . Moss temperatures were not measured but the predictions can be realistic given the level and diurnal amplitude of T_s in the organic layer (Fig. 6) beneath the mosses and soil heat flux G are reasonably reproduced (Fig. 5).

When the coupled soil and bryophyte energy and water balance sub-models are included, the APES can assist in the exploration of controls on bryophyte productivity and evaporation at different stands. Since hydraulic conductivity varies non-linearly with soil texture and water potential (Eq. (34)), interactions between

soil and bryophyte water balance are expected to be different at coarse and fine textured soils (or at sites with deep/shallow ground water level), which may have consequences on moss gas-exchange and productivity. Also, the importance of mosses as components of the carbon, water and energy balance, or their impact on soil micro-climate can also be addressed with such models. Further development is needed to incorporate accurate description of hydraulic characteristics and environmental controls of CO₂ uptake and respiration of different moss communities / species, and potentially hysteretic responses to desiccation (Silvolta, 1991; Schipperges and Rydin, 1998).

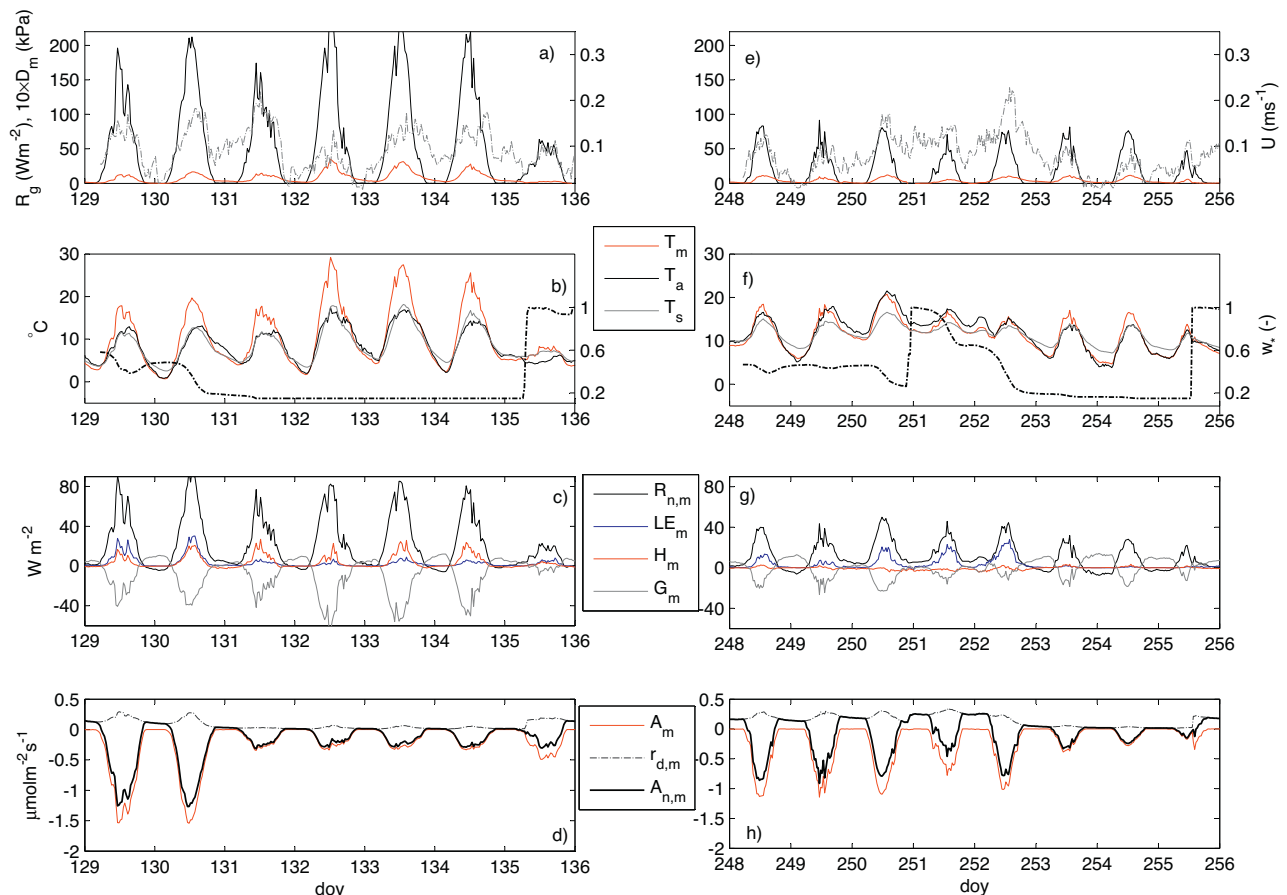


Fig. 11. Moss layer state variables and fluxes during one-week periods in May (left) and in September (right). Shown are global radiation (R_g), vapor pressure deficit (D_m , red) and mean wind speed above the moss canopy (a, e); moss (T_m), air (T_a) and topsoil (T_s) temperature and moss relative water content w_m^* (b, f); energy balance (downward fluxes negative) (c, g) and moss net CO₂ exchange ($A_{n,m}$) separated to respiration (r_m) and assimilation (A_m) components (d, h). (For interpretation of the references to colour in this figure legend, the reader is referred to the web version of this article.)

5. Summary

A 1-D multi-layer, multi-species soil-vegetation-atmosphere transfer model labeled APES (Atmosphere-Plant Exchange Simulator) was developed and evaluated for a well instrumented boreal pine forest across a wide range of hydroclimatic conditions. The APES is based on biophysical principles for upscaling CO₂, water, heat and momentum exchange from canopy element level to a stand scale. One of the main additions to earlier approaches is explicit description of the moss layer at the forest floor. When stand and soil characteristics were derived from measurements, and the functional descriptions of sub-models parametrized by literature values and shoot scale measurements, the model predicted observed fluxes of CO₂, H₂O and sensible heat and within-canopy scalar gradients both for diurnal and seasonal timescales. Also predictions for soil heat flux, soil temperature and moisture profiles and moss water storage dynamics were reasonable considering the heterogeneous forest soil and uncertainties in the boundary conditions.

The main novelties of the presented model framework are: (1) the full coupling between the above-ground and the soil domain through a feedback between soil water and vegetation, (2) the possibility of considering responses and resulting fluxes of different vascular plant species or age cohorts in a multi-species canopy (a feature not fully used in this study), (3) the explicit treatment of bryophyte layer energy and water balance and bottom layer – atmosphere exchange, which enables answering questions such as the role of bryophytes in stand water and carbon balance and soil environment, and (4) the object-oriented modeling approach and the stand-alone feature of many of the sub-models, both as model components and in their parametrization, which makes future development of APES efficient.

Acknowledgements

The staff of the Hytylä SMEAR II-station are acknowledged for their effort in maintenance of the long-term flux and environmental measurements, and numerous researchers who have contributed in measuring, quality-controlling and processing the field data. We acknowledge Dr. Liisa Kulmala for providing forest floor chamber fluxes and moss water content data and Dr. Tiia Grönholm for consultancy in numerical methods.

Appendix A. Nomenclature

Abbrev.	Units	Explanation
<i>Canopy structure, radiation transfer and interception</i>		
<i>z</i>	m	height above ground
<i>dz</i>	m	thickness of canopy a layer
<i>h</i>	m	stand height
$\Lambda_{l,t}(z)$	$m^2 m^{-3}$	stand leaf-area density profile
$F_{c,a}, F_{c,s}$	$\mu\text{mol m}^{-2} (\text{ground}) s^{-1}$	stand and sub-canopy net CO ₂ flux
LE_a, LE_s	$W m^{-2}$	stand and sub-canopy latent heat flux
H_a, H_s	$W m^{-2} (\text{ground})$	stand and sub-canopy sensible heat flux
<i>G</i>	$W m^{-2} (\text{ground})$	ground heat flux
S_s	$\text{mol m}^{-3} s^{-1} / W m^{-3}$	scalar sink/source term
K_s	$m^2 s^{-1}$	scalar eddy diffusivity
T_a	°C	air temperature
<i>U</i>	ms^{-1}	wind speed
c_p	$J mol^{-1} K^{-1}$	heat capacity of air at constant pressure
p_a	kPa	ambient pressure
Q_p	$\mu\text{mol m}^{-2} s^{-1}$	photosynthetically active radiation (PAR)
Q_n	$W m^{-2}$	near-infrared radiation (NIR)
Q_b	$W m^{-2}$	direct radiation
<i>PlantTypes</i>		
<i>LAI</i>	$m^2 m^{-2}$	hemi-surface leaf-area index
<i>WAI</i>	$m^2 m^{-2}$	woody-area index
$\Delta_l(z)$	$m^2 m^{-3}$	leaf-area density of <i>PlantType</i>
$\Delta_w(z)$	$m^2 m^{-3}$	woody-area density of <i>PlantType</i>
f_c	$\mu\text{mol m}^{-2} s^{-1}$	leaf net CO ₂ flux
f_e	$mmol m^{-2} s^{-1}$	leaf H ₂ O flux
f_h	$W m^{-2}$	leaf sensible heat flux
c_a	ppm	ambient CO ₂ mixing ratio
c_i	ppm	leaf internal CO ₂ mixing ratio
e_a	Pa	ambient vapor pressure
e_i	Pa	leaf internal vapor pressure
$e_s(T)$	Pa	saturation vapor pressure
<i>L</i>	$J mol^{-1}$	latent heat of vaporization
D_l	kPa	$D_l = e_s(T) - e_a$, vapor pressure deficit at surface temperature
A_p	$\mu\text{mol m}^{-2} s^{-1}$	Rubisco-limited photosynthetic rate
A_j	$\mu\text{mol m}^{-2} s^{-1}$	RuBP-regeneration (i.e. light) limited photosynthetic rate
r_d	$\mu\text{mol m}^{-2} s^{-1}$	leaf dark respiration rate
r_w	$\mu\text{mol m}^{-2} s^{-1}$	woody biomass respiration rate
V_{cmax}	$\mu\text{mol m}^{-2} s^{-1}$	maximum carboxylation velocity
J_{max}	$\mu\text{mol m}^{-2} s^{-1}$	maximum rate of electron transport
Γ^*	ppm	CO ₂ compensation point
a_1, a_2	ppm	Farquhar-model parameters
K_c	ppm	Michaelis constant for CO ₂
K_o	ppm	inhibition constant for O ₂
O_a	ppm	O ₂ mixing ratio in air
Θ	–	curvature of light response
γ	$mol mol^{-1}$	parameter related to quantum yield
$g_{b,i}$	$mol m^{-2} s^{-1}$	leaf boundary layer conductance
g_s	$mol m^{-2} s^{-1}$	stomatal conductance
g_v^*, g_c^*	$mol m^{-2} s^{-1}$	effective leaf conductances for H ₂ O and CO ₂
a_c	–	relative diffusivity of H ₂ O to CO ₂ in air (1.6)
$g_{1,ww}$	$kPa^{0.5}$	stomatal model slope in well-watered conditions
β_1	–	sensitivity of g_l to soil water potential
ψ_{pd}	m	predawn leaf water potential
ψ_r	m or MPa	root water potential

Abbrev.	Units	Explanation
$\psi_s(z)$	m or MPa	soil water potential
β_o	–	parameter of $V_{c,max}$ or J_{max} ψ_{pd} response
ψ_o	m or MPa	parameter of $V_{c,max}$ or J_{max} ψ_{pd} response
k_N	–	canopy nitrogen attenuation coefficient
T_r	ms^{-1}	transpiration rate of <i>PlantType</i>
R_i	ms^{-1}	root water uptake at layer i
g_{sr}^*	s^{-1}	soil to root conductance of H_2O
$R_{10,w}$	$\mu\text{mol m}^{-2} s^{-1}$	wood respiration rate at 10 °C
$Q_{10,w}$	–	temperature sensitivity of wood respiration
T_l	°C	leaf temperature
T_{lw}	°C	wet leaf temperature
<i>BottomLayer</i>		
LAI_m	$m^2 m^{-2}$	leaf area index of living bryophytes
T_m	°C	moss temperature
Δz_m	m	thickness of moss layer
l_m	m	characteristic roughness height of moss canopy
W_m	gg^{-1}	moss water content
W_*	–	water content relative to maximum
$W_{m,max}, W_{m,min}$	gg^{-1}	moss maximum and minimum water content
ψ_m	m or MPa	moss water potential
K_m	ms^{-1}	moss hydraulic conductivity
D_v	$m^2 s^{-1}$	molecular diffusivity of H_2O in air
$g_{b,m}$	$mol m^{-2} s^{-1}$	moss canopy boundary layer conductance of H_2O or heat
$g_{v,m}^*$	$mol m^{-2} s^{-1}$	moss canopy conductance for H_2O
λ_h	$Wm^{-1} K^{-1}$	thermal conductivity
$A_{n,m}$	$\mu\text{mol m}^{-2} s^{-1}$	moss net CO_2 exchange
$A_{m,max}$	$\mu\text{mol m}^{-2} s^{-1}$	maximum photosynthetic rate per unit leaf area
b	$\mu\text{mol m}^{-2} s^{-1}$	light half-saturation
r_m	$\mu\text{mol m}^{-2} s^{-1}$	moss respiration rate
E_m	$mmol m^{-2} s^{-1}$	moss evaporation rate
H_m	Wm^{-2}	moss-air sensible heat flux
G_m	Wm^{-2}	heat conduction between living bryophytes and top soil
I_m	Wm^{-2}	heat advection by precipitation
I_c	ms^{-1}	capillary water flux
<i>SoilProfile</i>		
z_s	m	depth below soil surface
Δz_s	m	thickness of a soil layer
T_s	°C	soil temperature
θ	$m^3 m^{-3}$	volumetric water content
θ_a	$m^3 m^{-3}$	air-filled porosity
θ_{sat}	$m^3 m^{-3}$	saturated water content
θ_{res}	$m^3 m^{-3}$	residual water content
S_e	–	saturation ratio
α, n, m	$m, -, -$	parameters of soil water retention curve
K_L	ms^{-1}	hydraulic conductivity
K_{Lsat}	ms^{-1}	saturated hydraulic conductivity
C_p	$J m^{-3} K^{-1}$	volumetric heat capacity of soil
c_w	$J g^{-1} K^{-1}$	specific heat of water
λ_h	$Wm^{-1} K^{-1}$	soil thermal conductivity
q_l	ms^{-1}	vertical liquid water flux
D	ms^{-1}	lateral subsurface flow
h_r	–	soil relative humidity
R_s	$\mu\text{mol m}^{-2} s^{-1}$	soil respiration rate
$R_{10,s}$	$\mu\text{mol m}^{-2} s^{-1}$	soil respiration rate at 10 °C
$Q_{10,s}$	–	temperature sensitivity of soil respiration
a, b, d, g	–	parameters of moisture sensitivity of R_s

Appendix B. Supplementary data

Supplementary data associated with this article can be found, in the online version, at <http://dx.doi.org/10.1016/j.ecolmodel.2015.06.007>.

References

- Aubinet, M., Vesala, T., Papale, D., 2012. *Eddy Covariance – A Practical Guide to Measurement and Data Analysis*, vol. 22. Springer.
- Baldocchi, D., 2008. Breathing of the terrestrial biosphere: lessons learned from a global network of carbon dioxide flux measurement systems. *Aust. J. Bot.* 56, 1–26.
- Baldocchi, D., Kelliher, F.M., Black, T.A., Jarvis, P., 2000. Climate and vegetation controls on boreal zone energy exchange. *Glob. Change Biol.* 6, 69–83.
- Baldocchi, D., Meyers, T., 1998. On using eco-physiological, micrometeorological and biogeochemical theory to evaluate carbon dioxide, water vapor and trace gas fluxes over vegetation: a perspective. *Agric. Forest Meteorol.* 90 (1–2), 1–25.
- Bengtsson, J., Nilsson, S.G., Franc, A., Menozzi, P., 2000. Biodiversity, disturbances, ecosystem function and management of European forests. *Forest Ecol. Manag.* 132 (1), 39–50.
- Beven, K., Germann, P., 1982. Macropores and water flow in soils. *Water Resour. Res.* 18 (5), 1311–1325.
- Bonan, G.B., 2008. Forests and climate change: forcings, feedbacks, and the climate benefits of forests. *Science* 320 (5882), 1444–1449.
- Bond-Lamberty, B., Gower, S.T., 2007. Estimation of stand-level leaf area for boreal bryophytes. *Oecologia* 151 (4), 584–592.
- Bouwer, H., Rice, R.C., 1984. Hydraulic properties of stony vadose zone. *Ground Water* 22 (6), 696–705.
- Campbell, G.S., Norman, J.M., 1998. *Introduction to Environmental Biophysics*, 2nd ed. Springer.
- Carleton, T., Dunham, K., 1996. Distillation in a boreal mossy forest floor. *Can. J. Forest Res.* 33, 663–671.
- Cescatti, A., 1997. Modelling the radiative transfer in discontinuous canopies of asymmetric crowns. 1. Model structure and algorithms. *Ecol. Model.* 101, 263–274.
- Cescatti, A., Zorer, R., 2003. Structural acclimation and radiation regime of silver fir (*Abies alba*) shoots along a light gradient. *Plant Cell Environ.* 26 (3), 429–442.
- Chapin, F.S., McGuire, A.D., Randerson, J., Pielke, R., Baldocchi, D., Hobbie, S.E., Roulet, N., Eugster, W., Kaschick, E., Rastetter, E.B., Zimov, S.A., Running, S.W., 2000. Arctic and boreal ecosystems of western North America as components of the climate system. *Glob. Change Biol.* 6, 211–223.
- Chuang, Y.-L., Bertozzi, R.O., Phillips, A.L., Katul, N.G.G., 2006. The porous media model for the hydraulic system of a conifer tree: linking sap flux data to transpiration rate. *Ecol. Model.* 191, 447–468.
- Couvreur, V., Vanderborght, J., Javaux, M., 2012. A simple three-dimensional macroscopic root water uptake model based on the hydraulic architecture approach. *Hydrolog. Earth Syst. Sci.* 16 (8), 2957–2971.
- Daamen, C., Simmonds, L., 1996. Measurement of evaporation from bare soil and its estimation using surface resistance. *Water Resour. Res.* 32, 1393–1402.
- de Vries, D.A., 1963. Thermal properties in soils. North Holland Pub. co., Amsterdam, pp. 210–235.
- Doussan, C., Pierret, A., Garrigues, E., Pags, L., 2006. Water uptake by plant roots. II: Modelling of water transfer in the soil root-system with explicit account of flow within the root system comparison with experiments. *Plant Soil* 283 (1–2), 99–117.
- Duursma, R.A., Kolari, P., Perämäki, M., Nikinmaa, E., Hari, P., Delzon, S., Loustau, D., Ilvesniemi, H., Pumpanen, J., Mäkelä, A., 2008. Predicting the decline in daily maximum transpiration rate of two pine stands during drought based on constant minimum leaf water potential and plant hydraulic conductance. *Tree Physiol.* 28 (2), 265–276.
- Egea, G., Verhoef, A., Vidale, P.L., 2011. Towards an improved and more flexible representation of water stress in coupled photosynthesis-stomatal conductance models. *Agric. Forest Meteorol.* 151, 1370–1384.
- Esseen, P.A., Ehnström, B., Ericson, L., Sjöberg, K., 1997. Boreal forest. *Ecol. Bull.* 46, 16–47.
- Farquhar, G.D., Caemmerer, S.V., Berry, J.A., 1980. A biochemical model for photosynthetic CO_2 assimilation in leaves of C3 species. *Planta* 149 (1), 78–90.
- Farquhar, G.D., von Caemmerer, S., Berry, J.A., 2001. Models of photosynthesis. *Plant Physiol.* 125 (1), 42–45.
- Finér, L., 1996. Variation in the amount and quality of litterfall in a *Pinus sylvestris* L. stand growing on a bog. *Forest Ecol. Manag.* 80, 1–11.
- Flerchinger, G.N., Xiao, W., Sauer, T.J., Yu, Q., 2009. Simulation of within-canopy radiation exchange. *NJAS – Wagening. J. Life Sci.* 57 (1), 5–15.
- Frolking, S., Goulden, M.L., Wofsy, S.C., Fan, S.-M., Sutton, D.J., Munger, J.W., Bazzaz, A.M., Daube, B.C., Crill, P.M., Aber, J.D., Band, L.E., Wang, X., Savage, K., Moore, T., Harris, R.C., 1996. Modelling temporal variability in the carbon balance of a spruce/moss boreal forest. *Glob. Change Biol.* 2 (4), 343–366.
- Gaalen, K.E.V., Flanagan, L.B., Peddle, D.R., 2007. Photosynthesis, chlorophyll fluorescence and spectral reflectance in Sphagnum moss at varying water contents. *Oecologia* 153 (1), 19–28.
- Gerdol, R., Iacumin, P., Marchesini, R., Bragazza, L., 2000. Water- and nutrient-use efficiency of a deciduous species, *Vaccinium myrtillus*, and an evergreen species,

- V. vitis-idaea*, in a subalpine dwarf shrub heath in the southern alps, Italy. *Oikos* 88, 19–32.
- Haataja, J., Vesala, T., 1997. SMEAR II: Station for Measuring Forest Ecosystem – Atmosphere Relation. University of Helsinki Department of Forest Ecology Publications, pp. 17.
- Hansson, K., Simunek, J., Mizoguchi, M., Lundin, L.C., van Genuchten, M.T., 2004. Water flow and heat transport in frozen soil: numerical solution and freeze-thaw applications. *Vadose Zone J.* 3 (2), 693–704.
- Hari, P., Kulmala, M., 2005. Station for measuring ecosystem-atmosphere relations (SMEAR II). *Boreal Environ. Res.* 10 (5), 315–322.
- Harley, P.C., Baldocchi, D.D., 1995. Scaling carbon-dioxide and water-vapor exchange from leaf to canopy in a deciduous forest 1. Leaf model parametrization. *Plant Cell Environ.* 18 (10), 1146–1156.
- Hölttä, T., Cochard, H., Nikinmaa, E., Mencuccini, M., 2009. Capacitive effect of cavitation in xylem conduits: results from a dynamic model. *Plant Cell Environ.* 32, 10–21.
- Ilvesniemi, H., Liu, C., 2001. Biomass distribution in a young Scots pine stand. *Boreal Environ. Res.* 6 (1), 3–8.
- Ilvesniemi, H., Pumpanen, J., Duursma, R., Hari, P., Keronen, P., Kolari, P., Kulmala, M., Mammarella, I., Nikinmaa, E., Rannik, Ü., Pohja, T., Siivola, E., Vesala, T., 2010. Water balance of a boreal Scots pine forest. *Boreal Environ. Res.* 15 (4), 375–396.
- Juang, J.-Y., Katul, G.G., Siqueira, M.B., Stoy, P.C., McCarthy, H.R., 2008. Investigating a hierarchy of Eulerian closure models for scalar transfer inside forested canopies. *Bound. Layer Meteorol.* 128 (1), 1–32.
- Kattge, J., Diaz, S., Lavelle, S., et al., 2011. TRY – a global database of plant traits. *Glob. Change Biol.* 17 (9), 2905–2935.
- Katul, G., Manzoni, S., Palmroth, S., Oren, R., 2010. A stomatal optimization theory to describe the effects of atmospheric CO₂ on leaf photosynthesis and transpiration. *Ann. Bot.* 105 (3), 431–442.
- Katul, G.G., Oren, R., Manzoni, S., Higgins, C., Parlange, M.B., 2012. Evapotranspiration: a process driving mass transport and energy exchange in the soil-plant-atmosphere-climate system. *Rev. Geophys.* 50, RG3002.
- Keenan, T., Sabate, S., Garcia, C., 2010. Soil water stress and coupled photosynthesis-conductance models: bridging the gap between conflicting reports on the relative roles of stomatal, mesophyll conductance and biochemical limitations to photosynthesis. *Agric. Forest Meteorol.* 150, 443–453.
- Keim, R., Skagset, A., Weiler, M., 2006. Storage of water on vegetation under simulated rainfall of varying intensity. *Adv. Water Resour.* 29, 974–986.
- Kellomäki, S., Hari, P., 1976. Rate of photosynthesis of some forest mosses as a function of temperature and light intensity and effect of water content of moss cushion on photosynthetic rate. *Silva Fennica* 10 (4), 288–295.
- Kellomäki, S., Wang, K.Y., 1996. Photosynthetic responses to needle water potentials in Scots pine after a four-year exposure to elevated CO₂ and temperature. *Tree Physiol.* 16 (9), 765–772.
- Kellomäki, S., Wang, K.Y., 1997. Effects of long-term CO₂ and temperature elevation on crown nitrogen distribution and daily photosynthetic performance of Scots pine. *Forest Ecol. Manag.* 99 (3), 309–326.
- Kolari, P., Kulmala, L., Pumpanen, J., Launiainen, S., Ilvesniemi, H., Hari, P., Nikinmaa, E., 2009. CO₂ exchange and component CO₂ fluxes of a boreal Scots pine forest. *Boreal Environ. Res.* 14 (4), 761–783.
- Kolari, P., Pumpanen, J., Kulmala, L., Ilvesniemi, H., Nikinmaa, E., Grönholm, T., Hari, P., 2006. Forest floor vegetation plays an important role in photosynthetic production of boreal forests. *Forest Ecol. Manag.* 221 (1–3), 241–248.
- Kulmala, L., Launiainen, S., Pumpanen, J., Lankreijer, H., Lindroth, A., Hari, P., Vesala, T., 2008. H₂O and CO₂ fluxes at the floor of a boreal pine forest. *Tellus Ser. B: Chem. Phys. Meteorol.* 60 (2), 167–178.
- Kulmala, L., Pumpanen, J., Hari, P., Vesala, T., 2011. Photosynthesis of ground vegetation in different aged pine forests: effect of environmental factors predicted with a process-based model. *J. Veg. Sci.* 22 (1), 96–110.
- Lange, O.L., Green, A., Heber, U., 2001. Hydration-dependent photosynthetic production of lichens: what do laboratory studies tell us about field performance? *J. Exp. Bot.* 52 (363), 2033–2042.
- Launiainen, S., 2010. Seasonal and inter-annual variability of energy exchange above a boreal Scots pine forest. *Biogeosciences* 7 (12), 3921–3940.
- Launiainen, S., Katul, G.G., Grönholm, T., Vesala, T., 2013. Partitioning ozone fluxes between canopy and forest floor by measurements and a multi-layer model. *Agric. Forest Meteorol.* 173, 85–99.
- Launiainen, S., Katul, G.G., Kolari, P., Vesala, T., Hari, P., 2011. Empirical and optimal stomatal controls on leaf and ecosystem level CO₂ and H₂O exchange rates. *Agric. Forest Meteorol.* 151 (12), 1672–1689.
- Launiainen, S., Rinne, J., Pumpanen, J., Kulmala, L., Kolari, P., Keronen, P., Siivola, E., Pohja, T., Hari, P., Vesala, T., 2005. Eddy covariance measurements of CO₂ and sensible and latent heat fluxes during a full year in a boreal pine forest trunk-space. *Boreal Environ. Res.* 10 (6), 569–588.
- Launiainen, S., Vesala, T., Moelder, M., Mammarella, I., Smolander, S., Rannik, Ü., Kolari, P., Hari, P., Lindroth, A., Katul, G.G., 2007. Vertical variability and effect of stability on turbulence characteristics down to the floor of a pine forest. *Tellus Ser. B: Chem. Phys. Meteorol.* 59 (5), 919–936.
- Laurén, A., Heiskanen, J., 1997. Physical properties of the mor layer in a Scots pine stand. I. Hydraulic conductivity. *Can. J. Soil. Sci.* 77 (4), 627–634.
- Law, B.E., Falge, E., Gu, L., Baldocchi, D.D., Bakwin, P., Berbigier, P., Davis, K., Dolman, A.J., Falk, M., Fuentes, J.D., Goldstein, A., Granier, A., Grelle, A., Hollinger, D., Janssens, I.A., Jarvis, P., Jensen, N.O., Katul, G., Mahli, Y., Matteucci, G., Meyers, T., Monson, R., Munger, W., Oechel, W., Olson, R., Pilegaard, K., Paw, K.T., Thorsteinsson, H., Valentini, R., Verma, S., Vesala, T., Wilson, K., Wofsy, S., 2002. Environmental controls over carbon dioxide and water vapor exchange of terrestrial vegetation. *Agric. Forest Meteorol.* 113 (1–4), 97–120.
- Leuning, R., Kelliher, F.M., Depury, D.G.G., Schulze, E.D., 1995. Leaf nitrogen, photosynthesis, conductance and transpiration – scaling from leaves to canopies. *Plant Cell Environ.* 18 (10), 1183–1200.
- Liu, S., 1998. Estimation of rainfall storage capacity in the canopies of cypress wetlands and slash pine uplands in North-Central Florida. *J. Hydrol.* 207, 932–941.
- Lundell, R., Saarinen, T., Aström, H., Hänninen, H., 2008. The boreal dwarf shrub *Vaccinium vitis-idaea* retains its capacity for photosynthesis through the winter. *Botany* 86, 491–500.
- Mäkelä, J.M., Aalto, P., Jokinen, V., Pohja, T., Nissinen, A., Palmroth, S., Markkanen, T., Seitsonen, K., Lihavainen, H., Kulmala, M., 1997. Observations of ultrafine aerosol particle formation and growth in boreal forest. *Geophys. Res. Lett.* 24 (10), 1219–1222.
- Malhi, Y., Baldocchi, D.D., Jarvis, P.G., 1999. The carbon balance of tropical, temperate and boreal forests. *Plant Cell Environ.* 22 (6), 715–740.
- Mammarella, I., Launiainen, S., Grönholm, T., Keronen, P., Pumpanen, J., Rannik, Ü., Vesala, T., 2009. Relative humidity effect on the high-frequency attenuation of water vapor flux measured by a closed-path eddy covariance system. *J. Atmos. Oceanic Technol.* 26, 1856–1866.
- Manoli, G., Bonetti, S., Domec, J.-C., Putti, M., Katul, G., Marani, M., 2014. Tree root systems competing for soil moisture in a 3D soil plant model. *Adv. Water Resour.* 66, 32–42.
- Manzoni, S., Vico, G., Katul, G., Fay, P.A., Polley, H.W., Palmroth, S., Porporato, A., 2010. Optimizing stomatal conductance for maximum carbon gain under water stress: a meta-analysis across plant functional types and climates. *Funct. Ecol.*, <http://dx.doi.org/10.1111/j.1365-2435.2010.01822>
- Manzoni, S., Vico, G., Palmroth, S., Porporato, A., Katul, G., 2013. Optimization of stomatal conductance for maximum carbon gain under dynamic soil moisture. *Adv. Water Resour.* 62, 90–105.
- Markewitz, D., Devine, S., Davidson, E.A., Brando, P., Nepstad, D.C., 2010. Soil moisture depletion under simulated drought in the Amazon: impacts on deep root uptake. *New Phytol.* 187 (3), 592–607.
- Martin, T.A., Hinckley, T.M., Meinzer, F.C., Sprugel, D.G., 1999. Boundary layer conductance, leaf temperature and transpiration of *Abies amabilis* branches. *Tree Physiol.* 19, 435–443.
- Maykut, G.A., Church, P.F., 1973. Radiation climate of Barrow, Alaska, 1962–66. *J. Appl. Meteorol.* 12, 620–628.
- McCarter, C., Price, J., 2014. Ecohydrology of Sphagnum moss hummocks: mechanisms of capitula water supply and simulated effects of evaporation. *Ecohydrology* 7, 33–44.
- Medlyn, B.E., Badeck, F.W., Purdy, D.G.D., Barton, C.V.M., Broadmeadow, M., Ceulemans, R., Angelis, P.D., Forstreuter, M., Jach, M.E., Kellomäki, S., Laitat, E., Marek, M., Philippot, S., Rey, A., Strassemeyer, J., Laitinen, K., Liozon, R., Portier, B., Roberntz, P., Wang, K., Jarvis, P.G., 1999. Effects of elevated CO₂ on photosynthesis in European forest species: a meta-analysis of model parameters. *Plant Cell Environ.* 22 (12), 1475–1495.
- Medlyn, B.E., Dreyer, E., Ellsworth, D., Forstreuter, M., Harley, P.C., Kirschbaum, M.U.F., Roux, X.L., Montpied, P., Strassemeyer, J., Walcroft, A., Wang, K., Loustau, D., 2002. Temperature response of parameters of a biochemically based model of photosynthesis. II. A review of experimental data. *Plant Cell Environ.* 25 (9), 1167–1179.
- Medlyn, B.E., Duursma, R.A., Eamus, D., Ellsworth, D.S., Prentice, I.C., Barton, C.V.M., Crous, K.Y., Angelis, P.D., Freeman, M., Wingate, L., 2012. Reconciling the optimal and empirical approaches to modelling stomatal conductance. *Glob. Change Biol.* 18 (11), 3476–3476.
- Melkerud, P.A., Bain, D.C., Jongmans, A.G., Tarvainen, T., 2000. Chemical, mineralogical and morphological characterization of three podzols developed on glacial deposits in Northern Europe. *Geoderma* 94 (2–4), 125–148.
- Meyers, T., Baldocchi, D., 1988. A comparison of models for deriving dry deposition fluxes of O₃ and SO₂ to a forest canopy. *Tellus Ser. B: Chem. Phys. Meteorol.* 40B, 270–284.
- Mythen, R.B., Ross, J., Asrar, G., 1989. A review on the theory of photon transport in leaf canopies. *Agric. Forest Meteorol.* 45 (1–2), 1–153.
- Ni-Meister, W., Yang, W., Kiang, N.Y., 2010. A clumped-foliation canopy radiative transfer model for a global dynamic terrestrial ecosystem model. I: Theory. *Agric. Forest Meteorol.* 150 (7–8), 881–894.
- Niemelä, S., Räisänen, P., Savijärvi, H., 2001. Comparison of surface radiative flux parameterizations. Part I: Longwave radiation. *Atmos. Res.* 58, 1–18.
- Niinemets, Ü., 2002. Stomatal conductance alone does not explain the decline in foliar photosynthetic rates with increasing tree age and size in *Picea abies* and *Pinus sylvestris*. *Tree Physiol.* 22, 515–535.
- Niinemets, Ü., Kull, O., 1995. Effects of light availability and tree size on the architecture of assimilative surface in the canopy of *Picea abies*: variation in needle morphology. *Tree Physiol.* 15 (5), 307–315.
- O'Donnell, J.A., Romanovsky, V.E., Harden, J.W., McGuire, A.D., 2009. The effect of moisture content on the thermal conductivity of moss and organic soil horizons from black spruce ecosystems in interior Alaska. *Soil Science* 174 (12), 646–651.
- Oechel, W.C., Cleve, K.V., 1986. The role of Bryophytes in nutrient cycling in taiga, Vol. 57 of Forest ecosystems in the Alaskan taiga. Springer, Berlin/Heidelberg/New York, pp. 121–137.
- Ogée, J., Brunet, Y., 2002. A forest floor model for heat and moisture including a litter layer. *J. Hydrol.* 255, 212–233.
- Ogée, J., Brunet, Y., Loustau, D., Berbigier, P., Delzon, S., 2003. MuSICA, a CO₂, water and energy multilayer, multileaf pine forest model: evaluation from hourly to yearly time scales and sensitivity analysis. *Glob. Change Biol.* 9 (5), 697–717.

- Olchev, A., Ibrom, A., Ross, T., Falk, U., Rakkib, G., Radler, K., Grote, S., Kreilein, H., Gravenhorst, G., 2008. A modelling approach for simulation of water and carbon dioxide exchange between multi-species tropical rain forest and the atmosphere. *Ecol. Model.* 212 (1–2), 122–130.
- Porporato, A., Daly, E., Rodriguez-Iturbe, I., 2004. Soil water balance and ecosystem response to climate change. *Am. Nat.* 164 (5), 625–632.
- Pumpenan, J., Ilvesniemi, H., Hari, P., 2003. A process-based model for predicting soil carbon dioxide efflux and concentration. *Soil Sci. Soc. Am. J.* 67 (2), 402–413.
- Rice, S.K., 2012. The cost of capillary integration for bryophyte canopy water and carbon dynamics. *Lindbergia* 35, 53–62.
- Rice, S.K., Collins, D., Anderson, A.M., 2001. Functional significance of variation in bryophyte canopy structure. *Am. J. Bot.* 88 (9), 1568–1576.
- Rice, S.K., Schneider, N., 2004. Cushion size, surface roughness and the control of water balance and carbon flux in the cushion moss *Leucobryum glaucum* (Leucobryaceae). *Am. J. Bot.* 91 (8), 1164–1172.
- Schaap, M.G., van Genuchten, M.T., 2006. A modified Mualem-van Genuchten formulation for improved description of the hydraulic conductivity near saturation. *Vadose Zone J.* 5 (1), 27–34.
- Schipperges, B., Rydin, H., 1998. Response of *Sphagnum* species from contrasting microhabitats to tissue water content and repeated desiccation. *New Phytol.* 140 (4), 677–684.
- Schuepp, P.H., 1993. Tansley review no. 59. leaf boundary-layers. *New Phytol.* 125 (3), 477–507.
- Silvola, J., 1991. Moisture dependence of carbon dioxide exchange and its recovery after drying in certain boreal forest and peat mosses. *Lindbergia* 1, 5–10.
- Simunek, J., Hopmans, J.W., 2009. Modeling compensated root water and nutrient uptake. *Ecol. Model.* 220 (4), 505–521.
- Siqueira, M., Katul, G., Porporato, A., 2008. Onset of water stress, hysteresis in plant conductance, and hydraulic lift: scaling soil water dynamics from millimeters to meters. *Water Resour. Res.* 44 (1).
- Skopp, J., Jawson, M.D., Doran, J.W., 1990. Steady-state aerobic microbial activity as a function of soil water content. *Soil Sci. Soc. Am. J.* 54, 1619–1625.
- Skre, O., Oechel, W.C., 1981. Moss functioning in different taiga ecosystems in interior Alaska, USA. 1. Seasonal phenotypic and drought effects of photosynthesis and response patterns. *Oecologia* 48 (1), 50–59.
- Smith, W.K., Carter, G.A., 1988. Shoot structural effects on needle temperatures and photosynthesis in conifers. *Am. J. Bot.* 75 (4), 496–500.
- Smolander, H., Stenberg, P., 1996. Response of LAI-2000 estimates to changes in plant surface area index in a Scots pine stand. *Tree Physiol.* 16 (3), 345–349.
- Smolander, H., Stenberg, P., Linder, S., 1994. Dependence of light interception efficiency of Scots pine shoots on structural parameters. *Tree Physiol.* 14 (7–9), 971–980.
- Spracklen, D.V., Bonn, B., Carslaw, K.S., 2008. Boreal forests, aerosols and the impacts on clouds and climate. *Philos. Trans. R. Soc. A* 366 (1885), 4613–4626.
- Stoy, P.C., Street, L.E., Johnson, A.V., Prieto-Blanco, A., Ewing, S.A., 2012. Temperature heat flux and reflectance of common subarctic mosses and lichens under field conditions: might changes to community composition impact climate-relevant surface fluxes? *Arct. Antarct. Alp. Res.* 44 (4), 500–508.
- Tanaka, K., 2002. Multi-layer model of CO₂ exchange in a plant community coupled with the water budget of leaf surfaces. *Ecol. Model.* 147 (1), 85–104.
- Teske, M.E., Thistle, H.W., 2004. A library of forest canopy structure for use in interception modeling. *Forest Ecol. Manag.* 198 (1–3), 341–350.
- van Dam, J.C., Feddes, R.A., 2000. Numerical simulation of infiltration, evaporation and shallow groundwater levels with the Richards equation. *J. Hydrol.* 233 (1–4), 72–85.
- van Genuchten, M., 1980. A closed form equation for predicting the hydraulic conductivity of unsaturated soils. *Soil Sci. Soc. Am. J.* 44 (5), 892–898.
- Vargas, R., Baldocchi, D.D., Allen, M.F., Bahn, M., Black, T.A., Collins, S.L., Yuste, J.C., Hirano, T., Jassal, R.S., Pumpenan, J., Tang, J., 2010. Looking deeper into the soil: biophysical controls and seasonal lags of soil CO₂ production and efflux. *Ecol. Appl.* 20 (6), 1569–1582.
- Volpe, V., Marani, M., Albertson, J.D., Katul, G., 2013. Root controls on water redistribution and carbon uptake in the soil-plant system under current and future climate. *Adv. Water Resour.* 60, 110–120.
- Wang, K.Y., Kellomäki, S., Laitinen, K., 1996. Acclimation of photosynthetic parameters in Scots pine after three years exposure to elevated temperature and CO₂. *Agric. Forest Meteorol.* 82 (1–4), 195–217.
- Watanabe, T., Mizutani, K., 1996. Model study on micrometeorological aspects of rainfall interception over an evergreen broad-leaved forest. *Agric. Forest Meteorol.* 80 (2–4), 195–214.
- Williams, C.A., Reichstein, M., Buchmann, N., Baldocchi, D., Beer, C., Schwalm, C., Wohlfahrt, G., Hasler, N., Bernhofer, C., Foken, T., Papale, D., Schymanski, S., Schaefer, K., 2012. Climate and vegetation controls on the surface water balance: synthesis of evapotranspiration measured across a global network of flux towers. *Water Resour. Res.*, 48.
- Williams, T.G., Flanagan, L.B., 1996. Effect of changes in water content on photosynthesis, transpiration and discrimination against ¹³CO₂ and C¹⁸O¹⁶ in Pleurozium and Sphagnum. *Oecologia* 108 (1), 38–46.
- Williams, T.G., Flanagan, L.B., 1998. Measuring and modelling environmental influences on photosynthetic gas exchange in Sphagnum and Pleurozium. *Plant Cell Environ.* 21 (6), 555–564.
- Zha, T., Li, C., Kellomäki, S., Peltola, H., Wang, K.-Y., Zhang, Y., 2013. Controls of evapotranspiration and CO₂ fluxes from Scots pine by surface conductance and abiotic factors. *PLOS ONE* 8 (7).
- Zhao, W.G., Qualls, R.J., 2005. A multiple-layer canopy scattering model to simulate shortwave radiation distribution within a homogeneous plant canopy. *Water Resour. Res.* 41 (8), A08409.
- Zhou, S., Duursma, R.A., Medlyn, B.E., Kelly, J.W.G., Prentice, I.C., 2013. How should we model plant responses to drought? An analysis of stomatal and non-stomatal responses to water stress. *Agric. Forest Meteorol.* 182, 204–214.